# Mitochondrial pyruvate carrier is required for optimal brown fat thermogenesis

Vanja Panic[1], Stephanie Pearson[1], James Banks[1], Trevor S. Tippetts[2], Sanghoon Lee[1], Judith Simcox[1], Gisela Geoghegan[1], Claire Bensard[1], Tyler van Ry[1], Will L. Holland[2], Scott Summers[2], James Cox[1], Greg Ducker[1], Jared Rutter[1,4], Claudio J. Villanueva[1,3]

[1]Department of Biochemistry, University of Utah, Salt Lake City, UT, 84112, USA.
[2]Department of Nutrition and Integrative Physiology, University of Utah, Salt Lake City, UT, 84112, USA.
[3]Department of Integrative Biology and Physiology, University of California, Los Angeles, CA, 90095, USA.
[4]Howard Hughes Medical Institute, University of Utah, Salt Lake City, UT, 84112, USA.

Corresponding Author:
Claudio J. Villanueva
cvillanueva@ucla.edu

## Abstract

Brown adipose tissue (BAT) is composed of thermogenic cells that convert chemical energy into heat to help maintain a constant body temperature and counteract metabolic disease in mammals. The metabolic adaptations required for thermogenesis are not fully understood. Here we explore how steady state levels of metabolic intermediates are altered in brown adipose tissue in response to cold exposure. Transcriptome and metabolome analysis revealed changes in pathways involved in amino acid, glucose, and TCA cycle metabolism. Using isotopic labeling experiments, we found that activated brown adipocytes increased labeling of pyruvate and TCA cycle intermediates from $U^{13}C$-glucose. Although glucose oxidation has been implicated as being essential for thermogenesis, its requirement for efficient thermogenesis has not been directly tested. Here we show that mitochondrial pyruvate uptake is essential for optimal thermogenesis, as conditional deletion of *Mpc1* in brown adipocytes leads to impaired cold adaptation. Isotopic labeling experiments using $U^{13}C$-glucose showed that loss of MPC1 led to impaired labeling of TCA cycle intermediates, while labeling of glycolytic intermediates was unchanged. Loss of MPC1 in BAT increased 3-hydroxybutyrate levels in blood and BAT in response to the cold, suggesting that ketogenesis provides an alternative fuel source that partially compensates for impaired mitochondrial oxidation of cytosolic pyruvate. Collectively, these studies highlight that complete glucose oxidation is essential for optimal brown fat thermogenesis.

## Introduction

The ability to thermoregulate has allowed mammals to thrive in cold regions of the world. Brown adipose tissue (BAT) thermogenesis is an energy demanding process that has been key to the evolution and survival of mammals (Gaudry et al., 2019, Oelkrug et al., 2015, Barnett and Dickson, 1989). With the excess calorie intake associated with a western diet, mechanisms that promote energy expenditure in the cold will provide attractive therapeutic interventions to treating metabolic diseases associated with obesity (Cypess et al., 2009, Vijgen et al., 2011). Cold exposure triggers the activation of the sympathetic nervous system to secrete norepinephrine, which signals through the β3-adrenergic receptor (β3-AR) and stimulates production of cyclic AMP (cAMP) (Townsend and Tseng, 2014, Londos et al., 1985). cAMP promotes the activation of protein kinase A (PKA), which in turn upregulates transcription of thermogenic pathways and leads to the activation of lipolysis (Cannon and Nedergaard, 2004, Zhang et al., 2005). Free fatty acids released can directly activate Uncoupling Protein 1 (UCP1), which uncouples the electron transport chain to generate heat (Fedorenko et al., 2012, Klaus et al., 1991, Busiello et al., 2015). Cold exposure stimulates uptake of both glucose, TG-rich lipoproteins and free fatty acids from the blood (Labbe et al., 2015, Heine et al., 2018, Ferre et al., 1986). While the relative contribution and importance of FFA as a BAT fuel source has been extensively studied (Bartelt et al., 2011, Khedoe et al., 2015, Townsend and Tseng, 2014, Lee et al., 2015), our understanding of metabolic fate of glucose and the importance of its catabolism in thermogenesis *in vivo* remains unknown.

Human brown fat was only believed to be found in newborns, but now we appreciate that adults have brown adipose tissue, a discovery that was made through use of glucose tracer ($^{18}$F-fluorodeoxyglucose) and positron-emission tomographic and computed tomographic (PET–CT) scans (Cypess et al., 2009, Virtanen et al., 2009). In addition, it was previously recognized that cold exposure could lower blood glucose levels in adults (Martineau and Jacobs, 1989). The role of glucose uptake on metabolism has been explored *in vitro* using immortalized brown adipocytes where siRNAs targeting GLUT1, GLUT4, hexokinase, or pyruvate kinase (enzymes catalyzing the first and the last step of glycolysis) demonstrated the importance of glycolysis, as β3-AR agonist failed to increase glucose uptake and oxygen consumption in these cells (Winther et al., 2018). However, there is no adequate *in vivo* model demonstrating the importance of BAT glycolysis or glucose oxidation on adaptive thermogenesis. We will address this question *in vivo* by blocking pyruvate import into mitochondria of brown adipocytes by knocking out the mitochondrial pyruvate carrier (MPC).

MPC is a multimeric complex in the inner mitochondrial membrane that consists of MPC1 and MPC2 subunits (Bricker et al., 2012, Herzig et al., 2012, Schell et al., 2014). Deletion of either subunit leads to instability of a functional MPC complex. MPC links the end product of glycolysis to glucose oxidation by transporting pyruvate into the mitochondrial matrix (Mowbray, 1975). Loss of function studies targeting MPC1 or MPC2 has been shown to limit mitochondrial pyruvate transport in yeast, flies and

mammals (Herzig et al., 2012, Bricker et al., 2012). Once in the mitochondria, pyruvate is decarboxylated to acetyl-CoA for further processing in the TCA cycle to generate NADH and fuel ATP production by OXPHOS complexes. Alternatively, cytosolic pyruvate can be reduced to lactate by lactate dehydrogenase complex A (LDHA), a process commonly upregulated in cancer cells (Vander Heiden et al., 2009). While it is clear that cold exposure or direct stimulation of β3-AR stimulates glucose utilization by BAT in both humans (Cypess et al., 2009, Saito et al., 2009) and rodents (Mirbolooki et al., 2014, Vallerand et al., 1990), it is not clear how important glucose oxidation is during thermogenesis nor what the metabolic fate of glucose is in activated BAT. Recently, comparative metabolomics analysis has shown that activation of BAT led to increased levels of the TCA cycle intermediate succinate, however it's unclear whether glucose-derived TCA cycle intermediates are required for thermogenesis (Mills et al., 2018).

In this study we use comprehensive metabolomics analysis of BAT and serum from mice housed at different temperatures, to gain insight into the metabolic pathways altered with cold exposure. We find changes in glucose, amino acid, and TCA cycle intermediates in BAT. Using [U-$^{13}$C]-glucose, we found increased glycolytic and TCA cycle metabolism during BAT stimulation. To test whether glucose oxidation is required for thermogenesis, we generated mice lacking mitochondrial pyruvate carrier 1 subunit (MPC1) in brown adipose tissue. We found that mice lacking MPC1 in BAT are cold sensitive, indicating that pyruvate import into the mitochondria is essential for efficient thermogenesis. Furthermore, when we profiled serum and BAT metabolites of MPC1-null mice, and found elevated 3-hydroxybutyrate levels. Prior studies supporting a role for ketogenesis in thermogenesis, suggests an alternative carbon source that compensates for the loss of pyruvate transport. Together this study provides new insights into the metabolic fate of glucose in brown adipose tissue during activation of thermogenesis in response to acute cold exposure.

## Results

### Cold-induced changes in transcriptome and metabolite profiling of BAT

To systematically profile the transcriptional changes that are altered in response to acute cold exposure, we measured steady state levels of RNA in BAT from mice at room temperature (24°C) or cold (4°C) for five hours. We found that 1,907 transcripts were upregulated with cold exposure, while 3,273 were decreased (**Supplemental Table 1 and 2**). Hierarchical clustering and Principal Component Analysis (PCA) revealed that the gene expression patterns in cold room and room temperature exposed BATs form two distinctive and independent clusters (**Supplementary Fig. 1a, 1b**). Using Gene Set Enrichment Analysis (GSEA) we found that cold exposure stimulated distinct transcriptional changes in BAT that involve various aspects of metabolism. Notable changes include induction of glucose metabolic process, sphingolipid metabolism, amino acid metabolism, and cellular respiration, while pathways involved in cell cycle control, DNA repair, and glycoprotein metabolism were downregulated (**Fig. 1a-b**).

To test whether steady state levels of metabolic intermediates were altered, we used targeted GC-MS analysis to complete comprehensive metabolic profiling of BAT (**Fig. 1c**) and serum (**Fig. 1d**) from mice across different temperatures (30°C, 23°C, and 4°C). The BAT metabolome showed elevated levels of glycolytic intermediates, TCA cycle intermediates, ketone bodies, and branched chain amino acids when mice were challenged with the cold (**Fig. 1c**). Notably, amino acids like tyrosine, alanine, threonine, and tryptophan increased in BAT, while their levels decreased in serum with cold exposure. Perhaps BAT uptake could lead to their depletion in the blood. Similar to a recent report (Yoneshiro et al., 2019a), we observed that branched chain amino acids, including Valine, Leucine, and Isoleucine were elevated in BAT, while only Leucine and Valine were upregulated in serum (**Fig. 1c and 1d**). Notably, glucose and pyruvate levels in BAT were elevated in response to 4°C, while both glucose and pyruvate levels were similar between mice housed at 30°C and 23°C. This finding would suggest that there is an increase in the rate of pyruvate synthesis in response to the cold (**Fig. 1c**). A list of measured metabolites from BAT and serum are detailed in (**supplemental table 3-4**).

The observed transcriptional and metabolite changes point to a reliance on pathways involved in carbohydrate metabolism (**Fig. 2a**). This prompted further analysis of glucose catabolism in brown adipocytes under aerobic conditions in response to a β3-AR agonist CL-316,243 (**Fig. 2b**). *In vitro* tracing experiments using [U-$^{13}$C]-Glucose showed that activation of brown adipocytes treated with CL-316,243 had significant $^{13}$C-glucose-derived M+3 isotopologues of $^{13}$C-Pyruvate, $^{13}$C-Lactate and $^{13}$C-Glycerol-3-Phosphate. Differentiated brown adipocytes that were treated with CL-316,243 had more than 50% of pyruvate and lactate labeled. Surprisingly, there was little alanine labeling from [U-$^{13}$C]-glucose, despite the rise in M+3 $^{13}$C-Alanine in response to β3-AR

activation (**Fig. 2b**). During incubation with [U-$^{13}$C]-Glucose, there was depletion of M+6 glucose in the media after CL-316,243 administration, while M+3 pyruvate in the media increased, but did not respond to CL-316,243 treatment (**Supplemental Fig. 1c**). To test whether M+3 lactate derived from [U-$^{13}$C]-Glucose was being released into the media, we measured media M+3 lactate, and found that CL-316,243 increased the release of M+3 lactate into the media when compared to vehicle (**Supplemental Fig. 1c**). These results suggest that activation of thermogenesis in brown adipocytes leads to increased lactate synthesis and secretion.

To address whether conditions that increase oxidative metabolism correlate with MPC levels, we measured the expression of *Mpc1* and *Mpc2* in BAT of C57BL6 mice challenged with thermoneutrality (30°C) or cold exposure (4°C) for 1-day or 1-week. Using real-time PCR, we found that both *Mpc1* and *Mpc2* expression had increased in BAT (**Fig. 3a**). This was accompanied by induction of thermogenic transcripts, including *Ucp1* and *Dio2*, while *Cidea* expression was unchanged (**Fig. 3a**). Similarly, we saw increased protein expression of MPC1, MPC2, and UCP1 in BAT after 1-week of cold exposure (**Fig. 3b**). In contrast, another mitochondrial protein, Cytochrome C, remained unchanged after a similar cold exposure. The increased expression of MPC1 may provide additional pyruvate transport and oxidative capacity for sustaining prolonged thermogenesis in BAT.

**BAT-selective deletion of *Mpc1* leads to cold sensitivity and impaired glucose handling**

To test whether MPC is required for thermogenesis we generated mice with conditional deletion of *Mpc1* in BAT by crossing *Mpc1*$^{F/F}$ mice(Gray et al., 2015) with UCP1-Cre(Kong et al., 2014) transgenic mice to generate *Mpc1*$^{F/F\ UCP1Cre}$ mice. The conditional deletion of *Mpc1* in brown adipose tissue was confirmed by gene expression analysis (**Fig. 3c**). To test whether loss of MPC1 resulted in destabilization of MPC2, we completed western blot analysis and found that MPC2 was also depleted in BAT of *Mpc1*$^{F/F\ UCP1Cre}$ mice (**Fig. 3d**). To address whether loss of MPC1 and MPC2 was specific to brown adipose tissue, we also completed western blot analysis on iWAT, and found similar levels of both MPC1 and MPC2 (**Fig. 3e**). To test whether MPC1 is required for thermogenesis, we completed a cold tolerance test at 4°C and measured core body temperature. Upon 5 hours of cold exposure, *Mpc1*$^{F/F\ UCP1Cre}$ mice had significantly lower core body temperatures when compared to their *Mpc1*$^{F/F}$ littermate controls, suggesting that mitochondrial pyruvate transport is essential for optimal thermogenesis (**Fig. 3f**). The cold sensitivity was not due to depletion of glucose, as blood glucose levels were similar between *Mpc1*$^{F/F}$ and *Mpc1*$^{F/F\ UCP1Cre}$ mice (**Supplemental Fig. 3a**).

To determine whether loss of MPC1 led to changes in systemic glucose metabolism, we completed a glucose tolerance test at room temperature (23°C) or with cold (4°C), and found that *Mpc1*$^{F/F\ UCP1Cre}$ mice had glucose excursion curves that were impaired when compared to their *Mpc1*$^{F/F}$ littermate controls (**Fig. 4a**). The loss of MPC1 in BAT did not change body composition of chow-fed mice (**Supplemental Fig. 4a**). We also found

that CL-316,243 administration resulted in a greater decrease in blood glucose levels in *Mpc1*$^{F/F}$ controls when compared to *Mpc1*$^{F/F\ UCP1Cre}$ mice (**Supplemental Fig. 4b**). In contrast, insulin sensitivity was similar between the two groups as demonstrated by % change in glucose over time (**Fig. 4b**). Histological analysis by H&E staining of BAT, iWAT, eWAT, and liver showed little to no differences in tissue morphology between the control and MPC1 null mice (**Fig. 4c**). Given that *Mpc1*$^{F/F\ UCP1Cre}$ mice had a cold sensitive phenotype, we measured gene expression of thermogenic-associated transcripts in BAT, and found that *Mpc1*$^{F/F\ UCP1Cre}$ mice had reduced expression of *UCP1*, *Dio2, Elovl3*, and *PPARγ* relative to *Mpc1*$^{F/F}$ control mice (**Fig. 4d**). No changes were observed in expression of genes involved in *de novo* lipogenesis and ketolysis (**Supplemental Fig. 3c**). To test whether there is compensation for loss of mitochondrial pyruvate uptake, we measured expression of genes that encode for transporters and enzymes involved in fatty acid oxidation. While we observed increased levels of the fatty acid transporter CD36 in *Mpc1*$^{F/F\ UCP1Cre}$ mice, we saw no differences in *ATGL*, *CPT1b*, *CPT2*, or *AGPAT* expression (**Fig. 4d**). This suggested that by gene expression, we do not see a compensatory upregulation of fatty acid oxidation in brown adipose tissue of mice lacking MPC1. We also did not find compensatory changes in thermogenic gene expression in iWAT (**Supplemental Fig. 3d**). In order to assess whether there is a difference in energy expenditure, food intake, or activity, we placed mice in Columbus Instruments Animal Monitoring System (CLAMS), and through continuous monitoring measured energy balance in mice challenged with 6°C. Although we did not find a significant reduction in energy expenditure with the loss of MPC1, RER was significantly elevated in *Mpc1*$^{F/F\ UCP1Cre}$ mice when compared to controls (**Fig. 3e-g**). Notably, both *Mpc1*$^{F/F}$ and *Mpc1*$^{F/F\ UCP1Cre}$ mice had reduction in RER, suggesting a metabolic switch towards fat utilization.

## Mitochondrial pyruvate transport is required to generate $^{13}$C-glucose-derived TCA cycle intermediates

While it is well established that cold exposure or CL-316,243 driven stimulation of β3-adrenergic receptor stimulates glucose uptake in brown adipose tissue, the metabolic fate of carbons from glucose has not been fully characterized. In order to assess how glucose is metabolized in control cells and those lacking MPC1, we retrovirally expressed MSCV-CreERT2 or empty MSCV control in *Mpc1*$^{F/F}$ brown preadipocytes to create a tamoxifen inducible knockout system. This allowed us to generate *Mpc1* nulls cells on day 1 of differentiation as confirmed by western blot (**Fig. 5a**) and gene expression analysis (**Fig. 5b**). Although *Mpc2* mRNA was not changed (**Fig. 5b**), loss of MPC1 led to destabilization and loss of MPC2 (**Fig. 5a**). First, we measured the [U-$^{13}$C]-Glucose-derived incorporation into the glycolysis intermediates (**Fig. 5c**). Similar to our previous results, we found that 5 hours of CL-316,243 stimulation leads to extensive M+3 labeling of pyruvate and lactate in both control and *Mpc1* null cells. Although labeling of alanine was limited, there was a noticeable CL-316,243 mediated induction of M+3 alanine, however loss of MPC1 showed similar incorporation relative to controls. Next, we measured $^{13}$C incorporation into TCA-cycle intermediates and found enrichment of $^{13}$C-glucose-derived TCA cycle metabolites in control cells treated with CL-316,243, which largely reflected the percent labeling of M+3 pyruvate and M+3

lactate (**Fig. 5d**). In contrast, MPC-null cells had impaired isotopic labeling of TCA cycle intermediates, including citrate/isocitrate, succinate, fumarate, and malate (**Fig. 5d**). This would suggest that MPC is necessary for β3-AR-driven glucose catabolism in brown adipocytes. Finally, to assess the impact of different fuels on oxygen consumption in brown adipocytes, we measure oxygen consumption on vehicle or CL-316,243 stimulated cells treated with either UK5099 (MPC inhibitor), etomoxir (CPT1 inhibitor), or both (**Fig. 5e**). We found that acute inhibition of pyruvate import with UK5099, resulted in elevated OCR in the basal state, an outcome that was not seen with etomoxir treatment. However, CL-316,243 administration increased OCR despite inhibition with UK5099 or etomoxir, while treatment with both UK5099/Etomoxir resulted in complete block of CL-316,243 stimulated oxygen consumption. We also found significant changes in basal respiration and proton leak that mirrored OCR (**Supplemental Fig. 4a)**. This would suggest that brown adipocytes are able to compensate when they lack one source of fuel but not both. Notably, we found both M+3 pyruvate and M+3 lactate in the media, particularly with the loss of MPC1 (**Supplemental Fig. 4a**). Upon stimulation with CL-316,243, we found greater levels of M+3 pyruvate and M+3 lactate in the media, with no distinguishable differences between control and knockout cells.

## Metabolic profiling shows increase in ketogenesis with loss of MPC in brown adipose tissue

To understand the systemic metabolic adaptations that occur with the loss of MPC in BAT, we completed metabolomics analysis of serum and BAT in cold challenged *Mpc1*$^{F/F}$ or *Mpc1*$^{F/F\ UCP1Cre}$ mice. We hypothesized that there may be compensatory mechanisms that allow *Mpc1*$^{F/F\ UCP1Cre}$ mice to cope with the loss of MPC during cold stress. Our metabolite analysis showed that cold exposed *Mpc1*$^{F/F\ UCP1Cre}$ mice had elevated 3-hydroxybutyrate, 2-hydroxybutyrate, adenosine 5'-monophosphate (AMP), 2-monopalmitoylglycerol, malonic acid, and cis-acotinic acid relative to *Mpc1*$^{F/F}$ mice (**Fig. 6a**). Analysis of the top 25 BAT metabolites showed a significant increase in 3-hydroxybutyrate, while TCA cycle intermediates such as succinic, citric, and isocitric acid were decreased (**Fig. 6b**). A list of measured metabolites in BAT and serum of *Mpc1*$^{F/F}$ or *Mpc1*$^{F/F\ UCP1Cre}$ mice are included in **Supplemental Table 3-4**. To test whether ketones were induced with cold exposure, we measured serum 3-hydroxybutyrate in *Mpc1*$^{F/F}$ and *Mpc1*$^{F/F\ UCP1Cre}$ mice, and found that cold exposure elevated serum 3-hydroxybutyrate levels in *Mpc1*$^{F/F}$ control mice (**Fig. 6c**). Notably, loss of MPC1 in brown adipose tissue led to blood 3-hydroxybutyrate levels that surpassed those of control mice in the cold (**Fig. 6c**). This prompted us to think that liver, being the major ketogenic organ, may be oxidizing more free fatty acids to produce 3-hydroxybutyrate as an alternative fuel for the extrahepatic organs during cold. Therefore, we examined the expression of genes implicated in fatty acid synthesis, oxidation, and ketone body production. While *FASN*, *ACC1,* and *Acly*, genes involved in fatty acid synthesis, were downregulated in *Mpc1*$^{F/F\ UCP1Cre}$ mice, *CPT1b*, *CPT2*, and *ACAD* (fatty acid oxidation genes) were increased, followed by increased levels of *HMGCS2* which is directly involved in ketogenesis (**Fig. 6d**). In contrast, upstream regulators of ketogenesis, including PPARα and Pgc1α, were not changed in the livers

(**Supplemental Figure 5a**). No notable differences were seen in serum free fatty acids (**Supplemental Figure 5b**), suggesting that activation of ketogenesis is likely contributing to rise in 3-hydroxybutyrate levels. Together, these findings suggest that activation of hepatic ketone production may provide a compensatory mechanism to counteract the inability to directly oxidize pyruvate in the BAT mitochondria.

## Discussion

There is a prevailing view that BAT relies primarily on FFAs as the primary source of energy for brown fat thermogenesis. However, it has been demonstrated in the past that cold activation of BAT leads to utilization of other substrates besides fatty acids, such as glucose, amino acids (Lopez-Soriano et al., 1988, Yoneshiro et al., 2019b) and acylcarnitines (Simcox et al., 2017). In this study we address a fundamental question in BAT thermogenesis: What is the role of glucose oxidation in short-term non-shivering thermogenesis? Is glycolysis or glucose-derived TCA cycle intermediates needed for efficient thermogenesis in BAT? Thus far, there have not been adequate *in vivo* models to answer these questions. In this study we combined *in vitro* U-$^{13}$C-glucose tracing experiments with comprehensive *in vivo* transcriptome and metabolome analysis of activated brown fat to address these questions.

Gene expression profiling of brown adipose tissue showed that mice exposed to short-term cold exposure exhibit evidence of activated cellular respiration, amino acid metabolism, and glucose metabolism. Similar, but distinct findings have been reported with prolonged cold exposure (2-4 days and 10 days respectively)(Hao et al., 2015, Rosell et al., 2014). In order to see how acute cold exposure affected the metabolome in mice, we followed up these studies by performing GC-MS metabolomics analysis on serum and BAT of mice housed at 30°C, 23°C, and 4°C for 5 hours. This analyses revealed increased branched chain amino acids, ketones, glucose, and TCA cycle metabolites in BAT with decreased temperatures. These results confirmed the previously proposed idea that BAT is a highly metabolically active tissue that upregulates uptake of various fuels to support the energy demand needed to adapt during cold stress. When stimulated with CL-316,243 for 5 hours and given [U-$^{13}$C]-labeled glucose, brown adipocytes significantly upregulated $^{13}$C incorporation into pyruvate, lactate, and TCA cycle intermediates, suggesting that glucose catabolism occurs early in BAT activation. These results are an important complement to recent studies that have described the metabolic response to chronic cold exposure (Hao et al., 2015, Marcher et al., 2015, Rosell et al., 2014). It is not surprising that acute activation of BAT leads to uptake of most substrates available to fuel the heat production process as an initial response to the cold shock. In contrast, cold acclimation or chronic exposure, leads to BAT remodeling and adaptive changes such as increased BAT mass, blood flow, and increased mitochondrial number(Lopez-Soriano et al., 1988, Rafael et al., 1985). Our observation that branched chain amino acids (BCAA) are elevated in BAT with cold exposure is consistent with recent findings highlighting their requirement for optimal thermogenesis (Yoneshiro et al., 2019b).

Here we show that mitochondrial pyruvate transport, presumably by its utilization in the TCA cycle, is essential for efficient thermogenesis. In wild type mice challenged with short-term cold exposure, we observe higher levels of MPC1 and MPC2 in BAT compared to that of mice housed at thermoneutrality. We propose that the induction of MPC1 and MPC2 is an adaptive mechanism to increase oxidative capacity during prolonged cold exposure. The inability to directly import pyruvate into the mitochondria for further oxidation leads to hypothermia, an indication of impaired thermogenesis. This was observed in our MPC1$^{F/F}$ UCP1-Cre mouse model where animals had lower core body temperatures during the cold challenge. We also noted small but significant reductions in thermogenic gene expression (*UCP1*, *Dio2*, *Elovl3*, *PPARγ*), but there were no compensatory changes in BAT expression of genes required for fatty acid oxidation. However, we did note that loss of MPC leads to upregulation of CD36, which may drive increased fatty acid uptake during the cold (Bartelt et al., 2011). In addition, there may be compensation by activating pathways that involve glutamine oxidation, transamination of alanine to pyruvate in the mitochondria, glutamine anaplerosis *via* glutamate to α-ketoglutarate by glutaminase and glutamate dehydrogenase enzymes, or conversion of glutamine-derived malate to pyruvate by mitochondrial malic enzyme (Bender and Martinou, 2016, Gray et al., 2015, McCommis et al., 2015, Schell et al., 2014, Vacanti et al., 2014, Yang et al., 2014).

One striking feature observed with cold adaptation in *Mpc1*$^{F/F\ UCP1\text{-}Cre}$ mice and their littermate controls was elevated ketone levels in the blood. MPC1$^{F/F\ UCP1Cre}$ mice had significantly elevated serum 3-hydroxybutyrate levels after 6 hours of cold challenge, but there were no measurable differences between the two groups after 6 hours at room temperature. These changes were accompanied by elevated 3-hydroxybutyrate levels in the BAT. Ketogenesis occurs primarily in the liver during exercise or prolonged fasting, and more recently was found to be a cold-induced metabolite(Newman and Verdin, 2014b, Newman and Verdin, 2014a, Wang et al., 2019). Ketones can be exported to extrahepatic tissues for further oxidation as they are rich energy sources. When we measured ketogenic gene expression in the liver, we found that *Mpc1*$^{F/F\ UCP1Cre}$ mice had significantly increased HMGCS2 levels compared to control mice. Together with serum and BAT metabolomics data this suggest that *Mpc1*$^{F/F\ UCP1Cre}$ mice compensate by activating ketone production. At first, we speculated that 3-hydroxybutyrate is utilized by BAT of *Mpc1*-deficient mice to compensate for the inability to oxidize pyruvate. However, in order for ketones to be catabolized in peripheral tissues they have to utilize OXCT1 for import and succinyl-CoA to donate coenzyme-A. In the BAT metabolomics analysis, MPC1$^{F/F\ UCP1Cre}$ mice had lower levels of TCA cycle intermediates compared to their littermate controls, including succinic acid, citric acid, and malic acid. This would suggest that oxidative metabolism is limited in the absence of MPC1. Further, this poses a question of why would MPC1$^{F/F\ UCP1Cre}$ mice make more 3-hydroxybutyrate and what role it might have in these mice? One likely explanation is that BAT utilizes ketones for thermogenesis. Alternatively, ketones can promote energy expenditure, mitochondrial biogenesis, and stimulate the expression of *Ucp1* in WAT(Srivastava et al., 2012).

Taken together, our studies aimed to gain a better understanding of the metabolic fate of glucose in BAT during short-term cold exposure. Here we report a novel mouse model of *Mpc1* loss in brown adipocytes that allowed us to assess the importance of efficient pyruvate import and oxidation for thermogenesis. Understanding the metabolic pathways and key metabolites that are upregulated in brown fat during cold exposure could provide new therapeutic targets to treat metabolic disorders such as obesity and diabetes.

## Methods

### Animals

All procedures were approved by the Institutional Animal Care and Use Committee (IACUC) of University of Utah. Mice were housed at 22°C-23°C using a 12 hr light/12 hr dark cycle. Animals were maintained on a regular Chow diet (2920x-030917M). Mice had ad libitum access to water at all times. Food was only withdrawn during experiments. C57BL6J male mice at 3 months of age were purchased from Jackson Laboratories. $MPC1^{F/F}$ mice were generated as previously described (Birsoy et al., 2015). Floxed mice were crossed with mice expressing UCP1-Cre (Jax #024670) to generate conditional mouse model. Floxed Cre-negative mice were used as wild-type controls. The age of mice used for all the studies were 12-20 weeks old. No animals were excluded from any experiments.

### Cold Exposure

For short-term cold exposure studies (5-6 hours) mice were single housed with no food, no bedding, with ad libitum access to water. Starting at T0 mice were placed at either 30°C (thermoneutrality), 23°C (room temperature), or 4-6°C (cold exposure) for 6 hrs. Body temperatures were taken once every hour with a physitemp A590 rectal probe using an Oaklon Thermocouple digital thermometer. For long-term cold exposure studies (1 week) mice were single housed, with bedding and ad libitum access to food and water.

### Glucose Tolerance and Insulin Tolerance Tests

For glucose tolerance test 12 weeks old mice were fasted for 6 hours and then administered 1g/kg of body weight of glucose by intraperitoneal injection. For insulin tolerance test non-fasted mice were administered 0.75 units/kg of body weight of insulin. Glucose levels were measured by tail vein using Contour next one glucometers at the indicated time points.

### Metabolic Cages

Food and water intake, energy expenditure and ambulatory activity were measured by using Comprehensive Lab Animal Monitoring System (CLAMS) (Columbus Instruments). Mice were single housed in metabolic cages with ad libitum access to

food and water on a 12 hr light/12 hr dark cycle. Temperature was initially set at 30°C, measurements were obtained for a period of 24 hours after which the temperature was decreased to 23°C for another 24 hours, after which it was switched to 7°C for 24 hrs. Energy expenditure was calculated as a function of oxygen consumption and carbon dioxide production in the CLAMS cages.

**CL-316,243 Treatment**

CL-316,243 (1mg/kg body weight; Sigma) or a vehicle control sterile PBS pH 7.4 was injected intraperitoneally. After drug or vehicle were administered, glucose levels were measured once every hour for 6 hours by tail vein using Contour next one glucometers. During this time mice were single housed at 23°C, with no food but water was readily available.

**Cell Culture**

Brown preadipocytes were isolated from 6-week old MPC1 F/F mice (Rodriguez-Cuenca et al., 2007). Intrascapular BAT was removed, minced, and digested in buffer containing 1% collagenase, DMEM (Cat# 11995073, Invitrogen Life) and antibiotics-50 IU Penicillin/mL and 50μg Streptomycin/mL (Cat# 15140122, Invitrogen Life) plus Primocin 100μg/mL (Cat# ANT-PM-2, Invivogen). Samples were incubated in the shaking water bath at 37°C for 45 minutes after which they were allow to cool on ice for 20 minutes. Infranatant was filtered through a 100μm filter and centrifuged for 5 minutes at 500xg. The digestion buffer was removed and pellet was washed twice with DMEM with antibiotics. After the last spin pellet was resuspended in 1 mL of DMEM containing 10% FBS (Cat# FB-01, Omega Scientific, Inc.) and antibiotics. Cells were then plated into a 6-well plate and the next day they were immortalized by retroviral expression of SV40 Large T-antigen (Cat# 13970, Adgene) using hygromycin for selection. For MPC1 null studies, stable expression of CreERT was generated using pMSCV CreERT2 retroviral vector (Cat# 22776, Adgene) with puromycin selection marker. For gene expression experiments, the cells were plated in 12-well plates (75,000 cells/well) in DMEM containing 10%FBS, 1nM T3 (Cat# T6397, Sigma), and 20nM insulin (Cat# 91077C, Sigma). Upon confluency cells were given differentiation cocktail containing 10%FBS, 1nM T3, 20nM insulin, 1μM rosiglitazone (Cat#71740, Cayman Chemical), 0.5μM dexamethasone (Cat# D4902, Sigma), 0.5mM isobutylmethylxanthine (Cat# I5879, Sigma), and 0.125mM indomethacin (Cat# I7378, Sigma). After 1 day of differentiation 100nM 4-hydroxy-tamoxifen (Cat# 3412, Tocris) was added to knock out MPC1 gene or DMSO (Cat# D2650, Sigma) was added as a control. After two days of differentiation, media was changed to DMEM containing 10% FBS, 1nM T3, 20nM insulin, and 1μM rosiglitazone. Cells were harvested on day 9 of differentiation for different experimental analyses.

**Brown Adipocyte U-$^{13}$C glucose and U-$^{13}$C palmitate labeling**

Cells were plated in a 6-well plate at a seeding density of 200,000 cells/well. On day 8 of differentiation cells were washed twice with 1XPBS and media was changed to high-glucose DMEM (Cat# 11995073, Thermo Fisher) containing 10% FBS overnight. The next day this media was removed and cells were washed twice with 1X PBS. They were incubated in a glucose/phenol red/glutamine free DMEM (Cat# A14430-01, Thermo

Fisher) with added 5.5mM glucose (Cat# G8270, Sigma), GlutaMax™(Cat# 35050061, Thermo Fisher), and MEM Non-Essential Amino Acid Solution (Cat# 11140050, Thermo Fisher). Cells were allowed to equilibrate for 4 hours before the media was changed to the same composed DMEM but this time containing 5.5mM U-$^{13}$C D-Glucose (Cat# CLM-1396-5, Cambridge Isotopes). For U-$^{13}$C palmitate labeling same composed media containing 5.5mM glucose was used with added 150μM U-$^{13}$C Sodium palmitate (CLM-6059-1, Cambridge Isotopes) conjugated to fatty acid free BSA (Cat# 700-107P, Gemini Bio Products) and 1mM Carnitine (Cat# C0823, Sigma). In both experiments cells were stimulated with 100nM CL-316,243 or vehicle for 5 hours. Before harvesting the cells 1mL od media was taken and centrifuged at 21,000xg for 10 minutes at 4°C. 40μL of supernatant were added to 160μL of ice-cold 80% methanol for metabolic tracing analysis. The remaining media was removed and cells were harvested by addition of 200μL of -80°C chilled buffer containing 20% water and 80% methanol (Cat# AA47192M6, Fisher Scientific). Lysed cells were kept on dry ice for 5 min before collection. Samples were spun down as before and 100μL of supernatant was directly used for metabolic tracer analysis.

**Measure of oxygen consumption**

Oxygen consumption rate was measured using a Seahorse XF96e analyzer. 35,000 differentiated brown adipocytes were plated in each well of a XF 96-well cell culture plate in 100μL of DMEM culture media and allowed to attach overnight. Cells were pre-treated overnight in vehicle or 10μM UK5099 and incubated at 37°C in 5% $CO_2$. Next day the culture media was replaced with standard assay media (DMEM, 25mM glucose, 1mM pyruvate, 2mM glutamine, pH 7.4). Cells were pretreated with 10μM Etomoxir for 15 minutes and activated with/without 100nM CL-316,243. Cells were run on a XF96e analyzer for a Mito Stress Test using manufacturers protocol and standard drug concentrations (Oligomycin 2.5μM, FCCP 2μM, Rotenone 0.5μM, and Antimycin A 0.5μM). Assay protocol was standard (3 measurements per phase, acute injection followed by 3 minutes of mixing, 0 minutes waiting, and 3 minutes measuring). Data was normalized to total cellular protein levels per well (ThermoFisher BCA Kit cat #23227).

**FFA measurement**

Free fatty acids were measured from the blood serum of MPC1 null mice and their littermate controls that were housed at room temperature or challenged by cold for 6 hours. 10 μL of the serum was used for analysis using commercial kit (Cat# MAK044-1KT, Sigma) according to the manufacturer instructions.

**Metabolite Extraction**

In order to extract metabolites from the tissue, each sample was transferred to 2.0ml ceramic bead mill tubes (bioExpress). Each sample received 450ul of 90% cold methanol in diH2O for every 25mg of tissue. The samples were then homogenized in an OMNI Bead Ruptor 24. Homogenized samples were then incubated at -20 ˚C for 1 hr. D4-succinic acid (Sigma 293075) was added to each sample as an internal standard. After incubation, all the samples were centrifuged at 20,000 x g for 10 minutes at 4˚C.

450ul of supernatant was then transferred from each bead mill tube into a labeled, fresh micro centrifuge tube where another internal standard d27-myristic acid (CDN Isotopes: D-1711). Samples were then dried *en vacuo.* For metabolite extraction from serum, 90% methanol in diH2O containing d4-succinic acid was added to each sample to give a final methanol concentration of 80%. Samples were vortexed and incubated at -20˚C for 1hr. After incubation, all samples were centrifuged at 20,000 x g for 10 minutes at 4˚C. Another internal standard, d27-myristic acid (CDN Isotopes: D-1711), was added to each sample. Process blanks were made using the extraction solvent and went through the same process steps as the real samples. The samples were then dried *en vacuo*.

**GC-MS analysis of metabolites**

All GC-MS analysis was performed with an Agilent 7200 GC-QTOF and an Agilent 7693A automatic liquid sampler. Dried samples were suspended in 40 µL of a 40 mg/mL O-methoxylamine hydrochloride (MOX) (MP Bio #155405) in dry pyridine (EMD Millipore #PX2012-7) and incubated for one hour at 37 °C in a sand bath. 25 µL of this solution was added to auto sampler vials. 60 µL of N-methyl-N-trimethylsilyltrifluoracetamide (MSTFA with 1%TMCS, Thermo #TS48913) was added automatically via the auto sampler and incubated for 30 minutes at 37 °C. After incubation, samples were vortexed and 1 µL of the prepared sample was injected into the gas chromatograph inlet in the split mode with the inlet temperature held at 250°C. A 5:1 split ratio was used for analysis for the majority of metabolites. Any metabolites that saturated the instrument at the 5:1 split were analyzed at a 50:1 split ratio. The gas chromatograph had an initial temperature of 60°C for one minute followed by a 10°C/min ramp to 325°C and a hold time of 10 minutes. A 30-meter Agilent Zorbax DB-5MS with 10 m Duraguard capillary column was employed for chromatographic separation. Helium was used as the carrier gas at a rate of 1 mL/min. Below is a description of the two step derivatization process used to convert non-volatile metabolites to a volatile form amenable to GC-MS. Pyruvic acid is used here as an example.

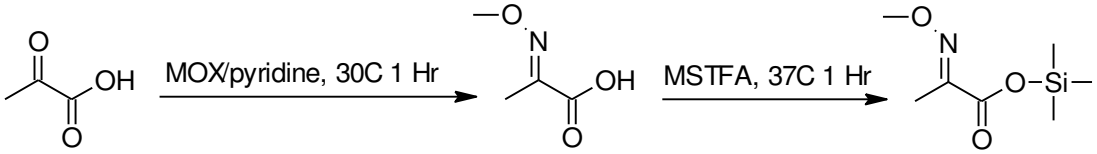


**Analysis of GC-MS metabolomics data**

Data was collected using MassHunter software (Agilent). Metabolites were identified and their peak area was recorded using MassHunter Quant. This data was transferred to an Excel spread sheet (Microsoft, Redmond WA). Metabolite identity was established using a combination of an in-house metabolite library developed using pure purchased standards, the NIST library and the Fiehn library. There are a few reasons a specific metabolite may not be observable through GC-MS. The metabolite may not be amenable to GC-MS due to its size, or a quaternary amine such as carnitine, or simply because it does not ionize well. Metabolites that do not ionize well include oxaloacetate, histidine and arginine. Cysteine can be observed depending on cellular conditions. It often forms disulfide bonds with proteins and is generally at a low concentration. Metabolites may not be quantifiable if they are only present in very low concentrations.

## LC-MS Metabolite Analysis

Extracted polar metabolite samples were analyzed by LC-MC. Separation was achieved by hydrophilic interaction liquid chromotograhpy (HILIC) using a Vanquish HPLC system (ThermoFisher Scientific). The column was an Xbridge BEH amide column (2.1 mm x 150mm, 2.5 µM particular size, 130Å pore size, Waters Co.) run with a gradient of solvent A (20 mM ammonium hydroxide, 20 mM ammonium acetate in 95:5 acetonitrile:Water, pH 9.5) and solvent B (100% acetonitrile) at a constant flow rate of 150 uL/min. The gradient function was: 0 min, 90% B; 2 min, 90% B; 3 min, 75% B; 7 min, 75% B; 8 min, 70% B; 9 min, 70% B; 10 min, 50% B; 12 min, 50% B; 13 min, 25% B; 14 min, 25% B; 16 min, 0% B; 20.5 min, 0% B; 21 min; 90% B; 25 min, 90% B. Autosampler temperature was 4°C, column temperature 30°C and injection volume 2 µL. Samples were injected by electrospray ionization into a QExactive HF orbitrap mass spectrometer (ThermoFisher Scientific) operating in negative ion mode with a resolving power of 120,000 at m/z of 200 and a full scan range of 75-1000. Data were analyzed using the MAVEN software package and specific peaks assigned based on exact mass and comparison with known standards (Melamud et al., 2010). Extracted peak intensities were corrected for natural isotopic abundance (Su et al., 2017).

## Gene Expression

RNA was isolated from differentiated brown adipocytes or from brown adipose tissue or white adipose tissue using Trizol reagent (Cat# 15596018, ThermoFisher). Tissue samples were homogenized with a TissueLyzer II (Qiagen). Isolated RNA was reverse transcribed using SuperScript VILO Mastermix (Cat# 11755500, ThermoFisher). Gene expression was quantified using Quant Studio 6 Flex Real-Time PCR instrument, 384-well (Applied Biosystems by Invitrogen) with KAPA SYBR FAST qPCR 2x Master Mix Rox Low (Cat# KK4621, Kapa Biosystems). Relative mRNA expression of indicated transcripts was normalized to expression of the housekeeping gene RPS3. Primers were designed using Universal Probe Library (Roche) or qPrimer Depot. A list of primer sequences can be found in **Supplementary Table 5**.

## Western Blots

Cells were lysed using Radioimmunoprecipitation assay (RIPA) buffer (Boston Bioproducts, Inc.) plus protease inhibitor cocktail (Cat# 04693124001, Sigma Aldrich) and phosphatase inhibitor cocktail (Cat# 78428, ThermoFisher). Lysates were passaged through a 25-gauge needle 10 times. Snap-frozen tissues were homogenized using a TissueLyzer II (Qiagen) in the same lysis buffer. Cell/tissue lysates were centrifuged twice at 13,000 rpm at 4°C for 10 minutes. Lipid layer was removed after each centrifugation. Protein concentrations were measured using Pierce BCA Protein Assay Kit (Cat# 23225, Thermo Fisher). 20µg of total protein was denatured using Laemmli buffer and samples were heated at 50°C for 10 minutes. Protein was loaded onto 10% acrylamide/bisacrylamide gels and transferred to a nitrocellulose membrane (GE Healthcare) for 60 minutes at 100 V for detection with the indicated antibodies. Briefly, membranes were blocked in 5% milk/PBST for 1 hr and then incubated with primary antibodies (1:1,000 dilution) in 5% BSA/PBST overnight at 4°C. Horse radish peroxidase-conjugated secondary antibodies (1:4,000 dilution) were given for 1 hr.

Western blots were developed using WesternSure Premium Chemiluminescent substrate (Cat# C807723-02, LI-COR Biosciences) and detected by ChemiDoc™ MP Imaging System (BioRad).

**Antibodies and Reagents**

MPC1 (14462), MPC2 (46141), β-Actin (4970), Akt (9272) were purchased from Cell Signaling Technologies, UCP1 (AB10983), Cytochrome C [7H8.2C12] (AB13575), HMGB1 (AB18256) were purchased from Abcam. 4-hydroxy-tamoxifen (4-OHT) and UK5099 were purchased from Tocris. CL-316,243 (C5796) was purchased from Sigma. U-$^{13}$C D-Glucose (CLM-1396-5) and U-$^{13}$C Sodium palmitate (CLM-6059-1) were purchased from Cambridge Isotopes. Sodium palmitate (P9767) was purchased from Sigma Aldrich. DL-[1-$^{14}$C] 3-hydroxybutyric acid sodium salt (ARC1455) was purchased from American Radiolabeled Chemicals. DL-β-Hydroxybutyric acid sodium salt (H6501) was purchased from Sigma.

**Quantification and Statistical Analysis**

Assessment of metabolomics t-test p-value, fold change, and generation of hierarchical clustering heat maps were performed in MetaboAnalyst 3.0 (Xia and Wishart, 2016). The data was interquartile range filtered, sum normalized, log2 transformed and autoscaled. Comparison of differentially abundant plasma or BAT metabolites from 3-month-old mice in 30°C, 23°C, or 4°C was performed in MetaboAnalyst 3.0 by using 1-way ANOVA analysis followed by Tukey's HSD post hoc test. All other data are presented as mean ± SEM and Student's t-test was used to determine significance, unless otherwise stated.

**RNA sequencing and data processing**

We used the standard procedure of Qiagen RNeasy kit to extract total RNA from BAT of mice. The RNA library for sequencing was prepared using TruSeq Stranded mRNA Library Prep Kit (Illumina , San Diego, CA, USA) and rRNA was removed by Ribo-Zero following the protocol provided by the manufacturer. The final libraries were normalized in preparation pooling by Kapa Library Quantification Kit for Illumina Platforms and the libraries were sequenced with the Illumina HiSeq 2000 sequencing platform within a lane for all six samples.For RNA-seq data process, we used Rsubread (Bioconductor release 3.8) [23558742] to align sequence reads to reference genome and used edgeR [22287627] and Limma [25605792] R packages (Bioconductor release 3.8) to normalize gene expression level to log2 transcripts per million (TPM) [22872506]. We aligned sequence reads to GRCh38 human genome reference sequence and mapped the aligned sequences to Ensembl or Entrez Gene IDs. After normalization for every sample, we used young room temperature (5 mice) and cold room exposed (5 mice) samples in this study. The raw RNA-seq data files and normalized expression profile data is available through GEO (GSEOOOOOO).

**Clustering analysis and Gene Set Enrichment Analysis (GSEA)**.

We removed genes of which expression level is zero across all samples and explored the expression clusters between young room temperature and cold room exposed

groups. We performed unsupervised hierarchical clustering analysis and Principal Component Analysis (PCA). We used Euclidean distance metric in hierarchical clustering, and the first three components in PCA. Furthermore, we validated this result with the supervised learning method, Random Forest. To identify biological processes whose expression differed between the clusters, we ran GSEA using Gene Ontology biological process (version 4.0) gene signatures [16199517]. In this analysis, we used all genes and calculated p-values by permuting the class labels 1000 times. Gene sets with a false discovery rate (FDR) q-value < 0.25 were considered significant. To visualize relationships among the top-performing gene signatures, we used EnrichmentMap [22962466].

## References

BARNETT, S. A. & DICKSON, R. G. 1989. Wild mice in the cold: some findings on adaptation. *Biol Rev Camb Philos Soc,* 64**,** 317-40.

BARTELT, A., BRUNS, O. T., REIMER, R., HOHENBERG, H., ITTRICH, H., PELDSCHUS, K., KAUL, M. G., TROMSDORF, U. I., WELLER, H., WAURISCH, C., EYCHMULLER, A., GORDTS, P. L., RINNINGER, F., BRUEGELMANN, K., FREUND, B., NIELSEN, P., MERKEL, M. & HEEREN, J. 2011. Brown adipose tissue activity controls triglyceride clearance. *Nat Med,* 17**,** 200-5.

BENDER, T. & MARTINOU, J. C. 2016. The mitochondrial pyruvate carrier in health and disease: To carry or not to carry? *Biochim Biophys Acta,* 1863**,** 2436-42.

BIRSOY, K., WANG, T., CHEN, W. W., FREINKMAN, E., ABU-REMAILEH, M. & SABATINI, D. M. 2015. An Essential Role of the Mitochondrial Electron Transport Chain in Cell Proliferation Is to Enable Aspartate Synthesis. *Cell,* 162**,** 540-51.

BRICKER, D. K., TAYLOR, E. B., SCHELL, J. C., ORSAK, T., BOUTRON, A., CHEN, Y. C., COX, J. E., CARDON, C. M., VAN VRANKEN, J. G., DEPHOURE, N., REDIN, C., BOUDINA, S., GYGI, S. P., BRIVET, M., THUMMEL, C. S. & RUTTER, J. 2012. A mitochondrial pyruvate carrier required for pyruvate uptake in yeast, Drosophila, and humans. *Science,* 337**,** 96-100.

BUSIELLO, R. A., SAVARESE, S. & LOMBARDI, A. 2015. Mitochondrial uncoupling proteins and energy metabolism. *Front Physiol,* 6**,** 36.

CANNON, B. & NEDERGAARD, J. 2004. Brown adipose tissue: function and physiological significance. *Physiol Rev,* 84**,** 277-359.

CYPESS, A. M., LEHMAN, S., WILLIAMS, G., TAL, I., RODMAN, D., GOLDFINE, A. B., KUO, F. C., PALMER, E. L., TSENG, Y. H., DORIA, A., KOLODNY, G. M. & KAHN, C. R. 2009. Identification and importance of brown adipose tissue in adult humans. *N Engl J Med,* 360**,** 1509-17.

FEDORENKO, A., LISHKO, P. V. & KIRICHOK, Y. 2012. Mechanism of fatty-acid-dependent UCP1 uncoupling in brown fat mitochondria. *Cell,* 151**,** 400-13.

776 FERRE, P., BURNOL, A. F., LETURQUE, A., TERRETAZ, J., PENICAUD, L., JEANRENAUD, B. &
777 GIRARD, J. 1986. Glucose utilization in vivo and insulin-sensitivity of rat brown adipose
778 tissue in various physiological and pathological conditions. *Biochem J,* 233**,** 249-52.
779 GAUDRY, M. J., CAMPBELL, K. L. & JASTROCH, M. 2019. Evolution of UCP1. *Handb Exp*
780 *Pharmacol,* 251**,** 127-141.
781 GRAY, L. R., SULTANA, M. R., RAUCKHORST, A. J., OONTHONPAN, L., TOMPKINS, S. C., SHARMA,
782 A., FU, X., MIAO, R., PEWA, A. D., BROWN, K. S., LANE, E. E., DOHLMAN, A., ZEPEDA-
783 OROZCO, D., XIE, J., RUTTER, J., NORRIS, A. W., COX, J. E., BURGESS, S. C., POTTHOFF, M.
784 J. & TAYLOR, E. B. 2015. Hepatic Mitochondrial Pyruvate Carrier 1 Is Required for
785 Efficient Regulation of Gluconeogenesis and Whole-Body Glucose Homeostasis. *Cell*
786 *Metab,* 22**,** 669-81.
787 HAO, Q., YADAV, R., BASSE, A. L., PETERSEN, S., SONNE, S. B., RASMUSSEN, S., ZHU, Q., LU, Z.,
788 WANG, J., AUDOUZE, K., GUPTA, R., MADSEN, L., KRISTIANSEN, K. & HANSEN, J. B. 2015.
789 Transcriptome profiling of brown adipose tissue during cold exposure reveals extensive
790 regulation of glucose metabolism. *Am J Physiol Endocrinol Metab,* 308**,** E380-92.
791 HEINE, M., FISCHER, A. W., SCHLEIN, C., JUNG, C., STRAUB, L. G., GOTTSCHLING, K., MANGELS,
792 N., YUAN, Y., NILSSON, S. K., LIEBSCHER, G., CHEN, O., SCHREIBER, R., ZECHNER, R.,
793 SCHEJA, L. & HEEREN, J. 2018. Lipolysis Triggers a Systemic Insulin Response Essential for
794 Efficient Energy Replenishment of Activated Brown Adipose Tissue in Mice. *Cell Metab,*
795 28**,** 644-655 e4.
796 HERZIG, S., RAEMY, E., MONTESSUIT, S., VEUTHEY, J. L., ZAMBONI, N., WESTERMANN, B., KUNJI,
797 E. R. & MARTINOU, J. C. 2012. Identification and functional expression of the
798 mitochondrial pyruvate carrier. *Science,* 337**,** 93-6.
799 KHEDOE, P. P., HOEKE, G., KOOIJMAN, S., DIJK, W., BUIJS, J. T., KERSTEN, S., HAVEKES, L. M.,
800 HIEMSTRA, P. S., BERBEE, J. F., BOON, M. R. & RENSEN, P. C. 2015. Brown adipose tissue
801 takes up plasma triglycerides mostly after lipolysis. *J Lipid Res,* 56**,** 51-9.
802 KLAUS, S., CASTEILLA, L., BOUILLAUD, F. & RICQUIER, D. 1991. The uncoupling protein UCP: a
803 membraneous mitochondrial ion carrier exclusively expressed in brown adipose tissue.
804 *Int J Biochem,* 23**,** 791-801.
805 KONG, X., BANKS, A., LIU, T., KAZAK, L., RAO, R. R., COHEN, P., WANG, X., YU, S., LO, J. C.,
806 TSENG, Y. H., CYPESS, A. M., XUE, R., KLEINER, S., KANG, S., SPIEGELMAN, B. M. &
807 ROSEN, E. D. 2014. IRF4 is a key thermogenic transcriptional partner of PGC-1alpha. *Cell,*
808 158**,** 69-83.
809 LABBE, S. M., CARON, A., BAKAN, I., LAPLANTE, M., CARPENTIER, A. C., LECOMTE, R. & RICHARD,
810 D. 2015. In vivo measurement of energy substrate contribution to cold-induced brown
811 adipose tissue thermogenesis. *FASEB J,* 29**,** 2046-58.
812 LEE, J., ELLIS, J. M. & WOLFGANG, M. J. 2015. Adipose fatty acid oxidation is required for
813 thermogenesis and potentiates oxidative stress-induced inflammation. *Cell Rep,* 10**,** 266-
814 79.
815 LONDOS, C., HONNOR, R. C. & DHILLON, G. S. 1985. cAMP-dependent protein kinase and
816 lipolysis in rat adipocytes. III. Multiple modes of insulin regulation of lipolysis and
817 regulation of insulin responses by adenylate cyclase regulators. *J Biol Chem,* 260**,** 15139-
818 45.

LOPEZ-SORIANO, F. J., FERNANDEZ-LOPEZ, J. A., MAMPEL, T., VILLARROYA, F., IGLESIAS, R. & ALEMANY, M. 1988. Amino acid and glucose uptake by rat brown adipose tissue. Effect of cold-exposure and acclimation. *Biochem J,* 252**,** 843-9.

MARCHER, A. B., LOFT, A., NIELSEN, R., VIHERVAARA, T., MADSEN, J. G., SYSI-AHO, M., EKROOS, K. & MANDRUP, S. 2015. RNA-Seq and Mass-Spectrometry-Based Lipidomics Reveal Extensive Changes of Glycerolipid Pathways in Brown Adipose Tissue in Response to Cold. *Cell Rep,* 13**,** 2000-13.

MARTINEAU, L. & JACOBS, I. 1989. Free fatty acid availability and temperature regulation in cold water. *J Appl Physiol (1985),* 67**,** 2466-72.

MCCOMMIS, K. S., CHEN, Z., FU, X., MCDONALD, W. G., COLCA, J. R., KLETZIEN, R. F., BURGESS, S. C. & FINCK, B. N. 2015. Loss of Mitochondrial Pyruvate Carrier 2 in the Liver Leads to Defects in Gluconeogenesis and Compensation via Pyruvate-Alanine Cycling. *Cell Metab,* 22**,** 682-94.

MELAMUD, E., VASTAG, L. & RABINOWITZ, J. D. 2010. Metabolomic analysis and visualization engine for LC-MS data. *Anal Chem,* 82**,** 9818-26.

MILLS, E. L., PIERCE, K. A., JEDRYCHOWSKI, M. P., GARRITY, R., WINTHER, S., VIDONI, S., YONESHIRO, T., SPINELLI, J. B., LU, G. Z., KAZAK, L., BANKS, A. S., HAIGIS, M. C., KAJIMURA, S., MURPHY, M. P., GYGI, S. P., CLISH, C. B. & CHOUCHANI, E. T. 2018. Accumulation of succinate controls activation of adipose tissue thermogenesis. *Nature,* 560**,** 102-106.

MIRBOLOOKI, M. R., UPADHYAY, S. K., CONSTANTINESCU, C. C., PAN, M. L. & MUKHERJEE, J. 2014. Adrenergic pathway activation enhances brown adipose tissue metabolism: a [(1)(8)F]FDG PET/CT study in mice. *Nucl Med Biol,* 41**,** 10-6.

MOWBRAY, J. 1975. A mitochondrial monocarboxylate transporter in rat liver and heart and its possible function in cell control. *Biochem J,* 148**,** 41-7.

NEWMAN, J. C. & VERDIN, E. 2014a. beta-hydroxybutyrate: much more than a metabolite. *Diabetes Res Clin Pract,* 106**,** 173-81.

NEWMAN, J. C. & VERDIN, E. 2014b. Ketone bodies as signaling metabolites. *Trends Endocrinol Metab,* 25**,** 42-52.

OELKRUG, R., POLYMEROPOULOS, E. T. & JASTROCH, M. 2015. Brown adipose tissue: physiological function and evolutionary significance. *J Comp Physiol B,* 185**,** 587-606.

RAFAEL, J., VSIANSKY, P. & HELDMAIER, G. 1985. Increased contribution of brown adipose tissue to nonshivering thermogenesis in the Djungarian hamster during cold-adaptation. *J Comp Physiol B,* 155**,** 717-22.

RODRIGUEZ-CUENCA, S., MONJO, M., FRONTERA, M., GIANOTTI, M., PROENZA, A. M. & ROCA, P. 2007. Sex steroid receptor expression profile in brown adipose tissue. Effects of hormonal status. *Cell Physiol Biochem,* 20**,** 877-86.

ROSELL, M., KAFOROU, M., FRONTINI, A., OKOLO, A., CHAN, Y. W., NIKOLOPOULOU, E., MILLERSHIP, S., FENECH, M. E., MACINTYRE, D., TURNER, J. O., MOORE, J. D., BLACKBURN, E., GULLICK, W. J., CINTI, S., MONTANA, G., PARKER, M. G. & CHRISTIAN, M. 2014. Brown and white adipose tissues: intrinsic differences in gene expression and response to cold exposure in mice. *Am J Physiol Endocrinol Metab,* 306**,** E945-64.

SAITO, M., OKAMATSU-OGURA, Y., MATSUSHITA, M., WATANABE, K., YONESHIRO, T., NIO-KOBAYASHI, J., IWANAGA, T., MIYAGAWA, M., KAMEYA, T., NAKADA, K., KAWAI, Y. &

TSUJISAKI, M. 2009. High incidence of metabolically active brown adipose tissue in healthy adult humans: effects of cold exposure and adiposity. *Diabetes,* 58**,** 1526-31.

SCHELL, J. C., OLSON, K. A., JIANG, L., HAWKINS, A. J., VAN VRANKEN, J. G., XIE, J., EGNATCHIK, R. A., EARL, E. G., DEBERARDINIS, R. J. & RUTTER, J. 2014. A role for the mitochondrial pyruvate carrier as a repressor of the Warburg effect and colon cancer cell growth. *Mol Cell,* 56**,** 400-13.

SIMCOX, J., GEOGHEGAN, G., MASCHEK, J. A., BENSARD, C. L., PASQUALI, M., MIAO, R., LEE, S., JIANG, L., HUCK, I., KERSHAW, E. E., DONATO, A. J., APTE, U., LONGO, N., RUTTER, J., SCHREIBER, R., ZECHNER, R., COX, J. & VILLANUEVA, C. J. 2017. Global Analysis of Plasma Lipids Identifies Liver-Derived Acylcarnitines as a Fuel Source for Brown Fat Thermogenesis. *Cell Metab,* 26**,** 509-522 e6.

SRIVASTAVA, S., KASHIWAYA, Y., KING, M. T., BAXA, U., TAM, J., NIU, G., CHEN, X., CLARKE, K. & VEECH, R. L. 2012. Mitochondrial biogenesis and increased uncoupling protein 1 in brown adipose tissue of mice fed a ketone ester diet. *FASEB J,* 26**,** 2351-62.

SU, X., LU, W. & RABINOWITZ, J. D. 2017. Metabolite Spectral Accuracy on Orbitraps. *Anal Chem,* 89**,** 5940-5948.

TOWNSEND, K. L. & TSENG, Y. H. 2014. Brown fat fuel utilization and thermogenesis. *Trends Endocrinol Metab,* 25**,** 168-77.

VACANTI, N. M., DIVAKARUNI, A. S., GREEN, C. R., PARKER, S. J., HENRY, R. R., CIARALDI, T. P., MURPHY, A. N. & METALLO, C. M. 2014. Regulation of substrate utilization by the mitochondrial pyruvate carrier. *Mol Cell,* 56**,** 425-35.

VALLERAND, A. L., PERUSSE, F. & BUKOWIECKI, L. J. 1990. Stimulatory effects of cold exposure and cold acclimation on glucose uptake in rat peripheral tissues. *Am J Physiol,* 259**,** R1043-9.

VANDER HEIDEN, M. G., CANTLEY, L. C. & THOMPSON, C. B. 2009. Understanding the Warburg effect: the metabolic requirements of cell proliferation. *Science,* 324**,** 1029-33.

VIJGEN, G. H., BOUVY, N. D., TEULE, G. J., BRANS, B., SCHRAUWEN, P. & VAN MARKEN LICHTENBELT, W. D. 2011. Brown adipose tissue in morbidly obese subjects. *PLoS One,* 6**,** e17247.

VIRTANEN, K. A., LIDELL, M. E., ORAVA, J., HEGLIND, M., WESTERGREN, R., NIEMI, T., TAITTONEN, M., LAINE, J., SAVISTO, N. J., ENERBACK, S. & NUUTILA, P. 2009. Functional brown adipose tissue in healthy adults. *N Engl J Med,* 360**,** 1518-25.

WANG, W., ISHIBASHI, J., TREFELY, S., SHAO, M., COWAN, A. J., SAKERS, A., LIM, H. W., O'CONNOR, S., DOAN, M. T., COHEN, P., BAUR, J. A., KING, M. T., VEECH, R. L., WON, K. J., RABINOWITZ, J. D., SNYDER, N. W., GUPTA, R. K. & SEALE, P. 2019. A PRDM16-Driven Metabolic Signal from Adipocytes Regulates Precursor Cell Fate. *Cell Metab,* 30**,** 174-189 e5.

WINTHER, S., ISIDOR, M. S., BASSE, A. L., SKJOLDBORG, N., CHEUNG, A., QUISTORFF, B. & HANSEN, J. B. 2018. Restricting glycolysis impairs brown adipocyte glucose and oxygen consumption. *Am J Physiol Endocrinol Metab,* 314**,** E214-E223.

XIA, J. & WISHART, D. S. 2016. Using MetaboAnalyst 3.0 for Comprehensive Metabolomics Data Analysis. *Curr Protoc Bioinformatics,* 55**,** 14 10 1-14 10 91.

YANG, C., KO, B., HENSLEY, C. T., JIANG, L., WASTI, A. T., KIM, J., SUDDERTH, J., CALVARUSO, M. A., LUMATA, L., MITSCHE, M., RUTTER, J., MERRITT, M. E. & DEBERARDINIS, R. J. 2014.

Glutamine oxidation maintains the TCA cycle and cell survival during impaired mitochondrial pyruvate transport. *Mol Cell,* 56**,** 414-24.

YONESHIRO, T., WANG, Q., TAJIMA, K., MATSUSHITA, M., MAKI, H., IGARASHI, K., DAI, Z., WHITE, P. J., MCGARRAH, R. W., ILKAYEVA, O. R., DELEYE, Y., OGURI, Y., KURODA, M., IKEDA, K., LI, H., UENO, A., OHISHI, M., ISHIKAWA, T., KIM, K., CHEN, Y., SPONTON, C. H., PRADHAN, R. N., MAJD, H., GREINER, V. J., YONESHIRO, M., BROWN, Z., CHONDRONIKOLA, M., TAKAHASHI, H., GOTO, T., KAWADA, T., SIDOSSIS, L., SZOKA, F. C., MCMANUS, M. T., SAITO, M., SOGA, T. & KAJIMURA, S. 2019a. BCAA catabolism in brown fat controls energy homeostasis through SLC25A44. *Nature,* 572**,** 614-619.

YONESHIRO, T., WANG, Q., TAJIMA, K., MATSUSHITA, M., MAKI, H., IGARASHI, K., DAI, Z., WHITE, P. J., MCGARRAH, R. W., ILKAYEVA, O. R., DELEYE, Y., OGURI, Y., KURODA, M., IKEDA, K., LI, H., UENO, A., OHISHI, M., ISHIKAWA, T., KIM, K., CHEN, Y., SPONTON, C. H., PRADHAN, R. N., MAJD, H., GREINER, V. J., YONESHIRO, M., BROWN, Z., CHONDRONIKOLA, M., TAKAHASHI, H., GOTO, T., KAWADA, T., SIDOSSIS, L., SZOKA, F. C., MCMANUS, M. T., SAITO, M., SOGA, T. & KAJIMURA, S. 2019b. BCAA catabolism in brown fat controls energy homeostasis through SLC25A44. *Nature*.

ZHANG, J., HUPFELD, C. J., TAYLOR, S. S., OLEFSKY, J. M. & TSIEN, R. Y. 2005. Insulin disrupts beta-adrenergic signalling to protein kinase A in adipocytes. *Nature,* 437**,** 569-73.

**Figure 1. Transcriptome and metabolomics analysis of brown fat shows increased carbohydrate metabolism and glycolytic metabolism during cold exposure.**

(a) Network visualization of enriched biological pathways altered with cold exposure in BAT (N=5).

(b) GSEA pathway analysis of differentially expressing genes (FDR<0.05) in BAT at 4°C versus room temperature (N=5).

(c-d) Heat map of relative normalized changes in BAT (c) and serum (d) metabolites at 30°C, 23°C, and 4°C. Dendograms illustrate hierarchical clustering of pattern similarity across metabolites (left) and conditions (top). Each column represents average within the group (N=5 per group). Data was sum normalized, log transformed, and autoscaled.

**Figure 2. Transcriptome and metabolomics analysis of brown fat shows increased carbohydrate metabolism during cold exposure.**

(a) Atom mapping for [U-$^{13}$C]glucose tracing into glycolysis and the TCA cycle. White balls are $^{12}$C atoms. Black balls are $^{13}$C atoms.

(b) Tracing analysis from U-$^{13}$C glucose in differentiated brown adipocytes treated with vehicle or 100nM CL-316,243 for 5 hours (N=3).

**Figure 3. Loss of MPC1 in BAT impairs thermogenesis and leads to cold sensitivity.**

(a) Relative gene expression in brown adipose tissue from mice adapted to 30°C or 4°C for 1 day or 1 week. N=4-5.

(b) Western blot analysis of brown adipose tissue of mice adapted to 30°C or 4°C for 1 week. N=4-5.

(c) Gene expression of MPC1 and MPC2 in brown adipose tissue after 6 hours of cold exposure. N=7.

(d) Western blot analysis of brown adipose tissue and white adipose tissue (e) at 4°C. N=4.

(f) Core body temperature during cold challenge at 4°C. N=7.

**Figure 4. Conditional deletion of *Mpc1* in BAT impairs systemic glucose metabolism.**

(a) Glucose tolerance test at room temperature (23°C) and cold (4°C) in *Mpc1*$^{F/F}$ and *Mpc1*$^{F/F\ UCP1Cre}$ 3-4 months old, N=5.

(b) Insulin tolerance test at room temperature (23°C) in *Mpc1*$^{F/F}$ and *Mpc1*$^{F/F\ UCP1Cre}$, 3-4 months old, N=6.

(c). Representative H&E images of BAT, iWAT, eWAT, and liver from *Mpc1*$^{F/F}$ and *Mpc1*$^{F/F\ UCP1\ Cre}$ mice exposed to 4°C for 6 hours.

(d) Gene expression in BAT from *Mpc1*$^{F/F}$ and *Mpc1*$^{F/F\ UCP1\ Cre}$ mice exposed to 4°C for 6 hours. N=6.

(e-h) Energy expenditure, RER, and locomotor activity of *Mpc1*$^{F/F}$ and *Mpc1*$^{F/F\ UCP1\ Cre}$ mice at 6°C. N=4.

**Figure 5. Mitochondrial pyruvate transport is required for $^{13}$C-glucose-derived TCA cycle intermediates**

(a) Western blot analysis of differentiated brown *Mpc1*$^{F/F}$ adipocytes expressing pMSCV2 or CreERT2 treated with ethanol or 4-hydroxy tamoxifen. N=3.

(b) Gene expression analysis in differentiated brown *Mpc1*$^{F/F}$ adipocytes expressing pMSCV2 or CreERT2 treated with ethanol or 4-hydroxy tamoxifen N=3

(c-d) U-$^{13}$C-glucose labeling in *Mpc1*$^{F/F}$ adipocytes expressing CreERT2 treated with ethanol or 4-hydroxy tamoxifen, with/without 100nM CL-316,243 for 5 hours (N=6).

(e) Oxygen consumption rate in differentiated brown adipocytes treated with/without 100nM CL-316,243 ± 10μM UK5099, 10μM Etomoxir, or both. (N=10-12).

**Figure 6. Conditional deletion of MPC1 in brown fat leads to increased ketogenesis.**

(a) Volcano plot showing changes in serum metabolites between *Mpc1*$^{F/F}$ and *Mpc1*$^{F/F\text{-}UCP1\ Cre}$ mice housed at 4°C for 6 hours. N=6.

(b) Heat map of top 25 metabolites in BAT from *Mpc1*$^{F/F}$ and *Mpc1*$^{F/F\ UCP1\ Cre}$ mice housed at 4°C for 6 hours. Dendograms illustrate hierarchical clustering across metabolites (left) and genotypes (top). N=6. Data was sum normalized, log transformed, and autoscaled.

(c) Serum 3-hydroxybutyrate levels from *Mpc1*$^{F/F}$ and *Mpc1*$^{F/F\ UCP1\ Cre}$ mice housed at 23°C or 4°C for 6 hours. N=6.

(d) Gene expression analysis of livers from *Mpc1*$^{F/F}$ and *Mpc1*$^{F/F\ UCP1\ Cre}$ mice housed at 4°C for 6 hours. N=6.

Supplemental Figure 1

(a) Hierarchical clustering illustrates large-scale differences in gene expression between cold room and room temperature exposed BAT.

(b) Unsupervised principal component analysis (PCA) shows that cold room and room temperature exposed BATs are separated and form distinctive clusters in principal components. The first three principal components were used to present the samples in the 3-dimentional PCA plot.
(c) $^{13}C$ labeling of M+6 glucose and M+3 pyruvate and lactate in the media of brown adipocytes treated with vehicle or 100nM CL-316,243 for 1 or 5 hours (N=3).
(d) Total intracellular pyruvate and lactate (M and M+3) of brown adipocytes treated with vehicle or 100nM CL-316,243 for 1 or 5 hours (N=3).

Supplemental Figure 2
(a) Blood glucose levels in *Mpc1*$^{F/F}$ and *Mpc1*$^{F/F\ UCP1\ Cre}$ mice exposed to 4°C for 6 hours (N=6).

Supplemental Figure 3
(a) Body composition of *Mpc1*$^{F/F}$ and *Mpc1*$^{F/F\ UCP1\ Cre}$ mice housed at room temperature by NMR.
(b) Time-dependent changes in blood glucose levels in *Mpc1*$^{F/F}$ and *Mpc1*$^{F/F\ UCP1\ Cre}$ mice mice 3-4 months old treated with 1mg/kg CL-316,243 (N=6).
(c) Gene expression in BAT from *Mpc1*$^{F/F}$ and *Mpc1*$^{F/F\ UCP1\ Cre}$ mice housed at 4°C for 6 hours.
(d) Gene expression in iWAT from *Mpc1*$^{F/F}$ and *Mpc1*$^{F/F\ UCP1\ Cre}$ mice housed at 4°C for 6 hours.

Supplemental Figure 4
(a) Seahorse analysis of basal respiration, proton leak, or ATP production in differentiated brown adipocytes treated with/without 100nM CL-316,243 ± 10μM UK5099, 10μM Etomoxir, or both. (N=10-12).
(b) Total media pyruvate and lactate from *Mpc1*$^{F/F}$ adipocytes expressing CreERT2 treated with ethanol or 4-hydroxy tamoxifen, with/without 100nM CL-316,243 for 5 hours in [U-$^{13}C$] glucose (N=6).

Supplemental Figure 5
(a) Gene expression in livers from *Mpc1*$^{F/F}$ and *Mpc1*$^{F/F\ UCP1\ Cre}$ mice housed at 4°C for 6 hours.
(b) Free fatty acid levels in serum of *Mpc1*$^{F/F}$ and *Mpc1*$^{F/F\ UCP1\ Cre}$ mice housed either at challenged with 4°C for 6 hours.
(c) Ketogenic gene expression in iWAT from *Mpc1*$^{F/F}$ and *Mpc1*$^{F/F\ UCP1\ Cre}$ mice housed at 4°C for 6 hours. Data was analyzed by Student's t-test. Values are shown as mean+s.e.m. (N=6).

1075

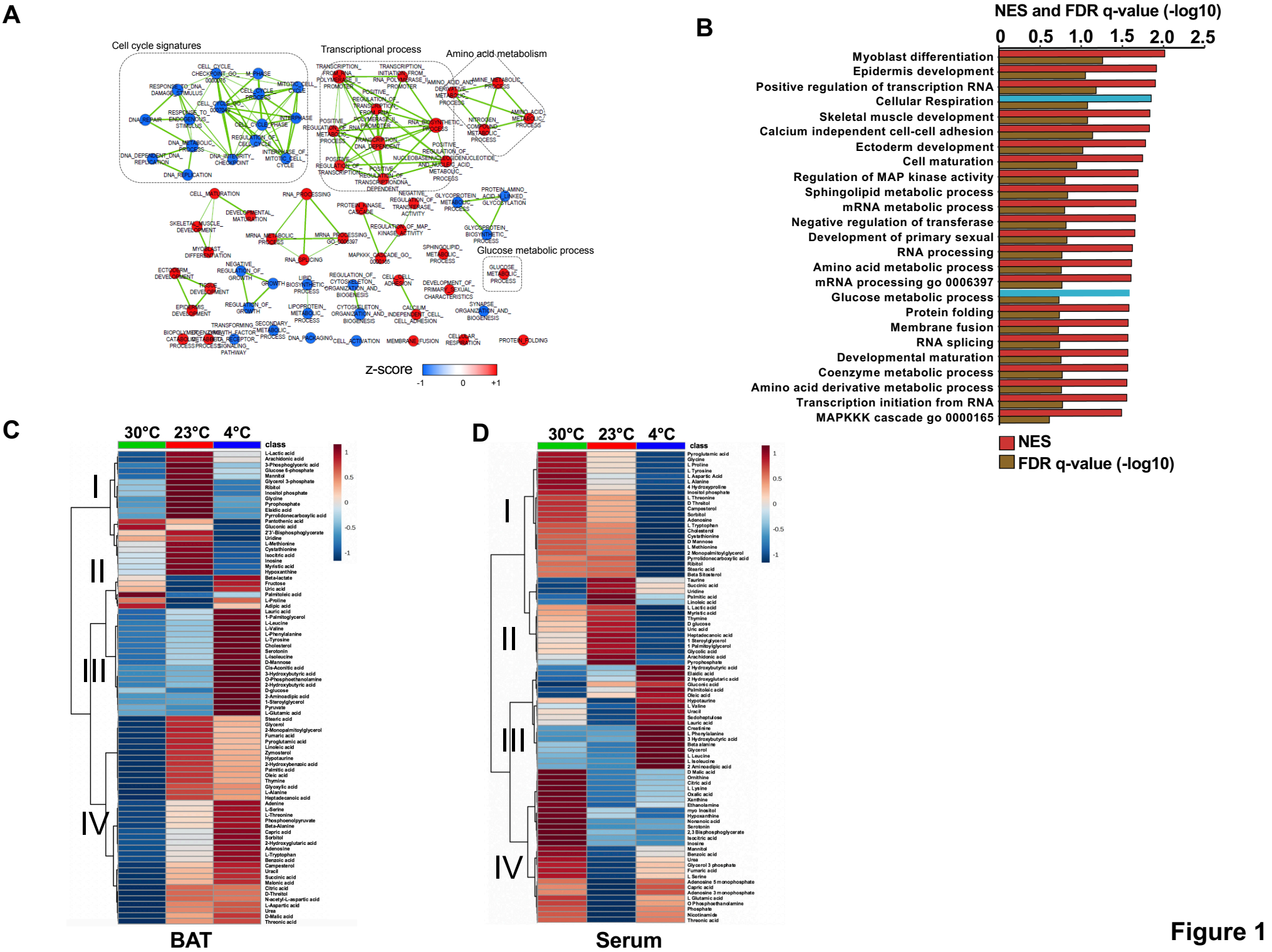
A
Cell cycle signatures
Transcriptional process
Amino acid metabolism
Glucose metabolic process
z-score
-1
0
+1
B
NES and FDR q-value (-log10)
0
0.5
1.0
1.5
2.0
2.5
Myoblast differentiation
Epidermis development
Positive regulation of transcription RNA
Cellular Respiration
Skeletal muscle development
Calcium independent cell-cell adhesion
Ectoderm development
Cell maturation
Regulation of MAP kinase activity
Sphingolipid metabolic process
mRNA metabolic process
Negative regulation of transferase
Development of primary sexual
RNA processing
Amino acid metabolic process
mRNA processing go 0006397
Glucose metabolic process
Protein folding
Membrane fusion
RNA splicing
Developmental maturation
Coenzyme metabolic process
Amino acid derivative metabolic process
Transcription initiation from RNA
MAPKKK cascade go 0000165
NES
FDR q-value (-log10)
C
30°C
23°C
4°C
class
I
II
III
IV
BAT
D
30°C
23°C
4°C
class
I
II
III
IV
Serum

Figure 1

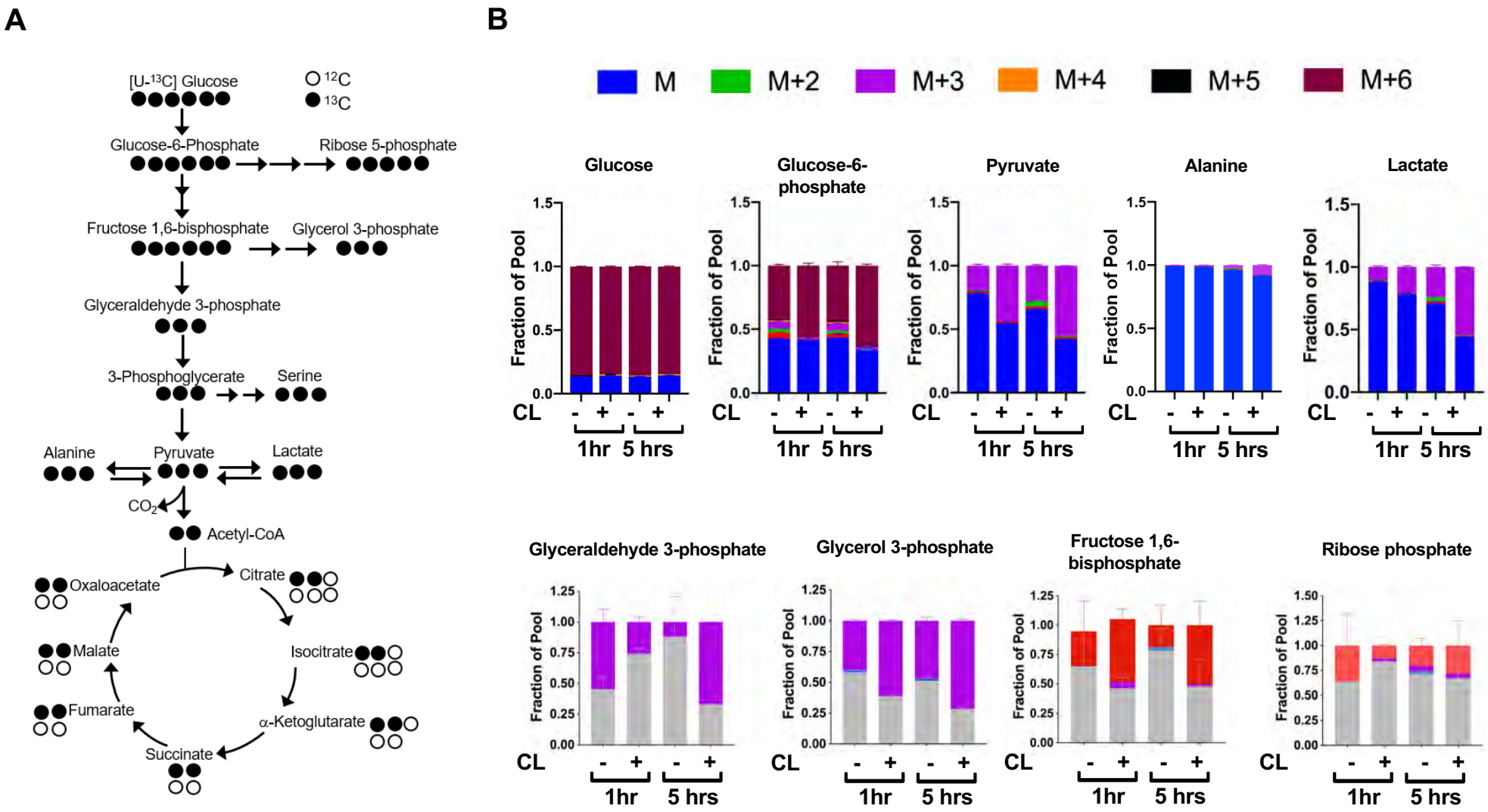
A
[U-13C] Glucose
12C
13C
Glucose-6-Phosphate
Ribose 5-phosphate
Fructose 1,6-bisphosphate
Glycerol 3-phosphate
Glyceraldehyde 3-phosphate
3-Phosphoglycerate
Serine
Alanine
Pyruvate
Lactate
CO2
Acetyl-CoA
Oxaloacetate
Citrate
Isocitrate
α-Ketoglutarate
Succinate
Fumarate
Malate
B
M
M+2
M+3
M+4
M+5
M+6
Glucose
Glucose-6-phosphate
Pyruvate
Alanine
Lactate
Glyceraldehyde 3-phosphate
Glycerol 3-phosphate
Fructose 1,6-bisphosphate
Ribose phosphate
Fraction of Pool
CL
1hr
5 hrs

Figure 2

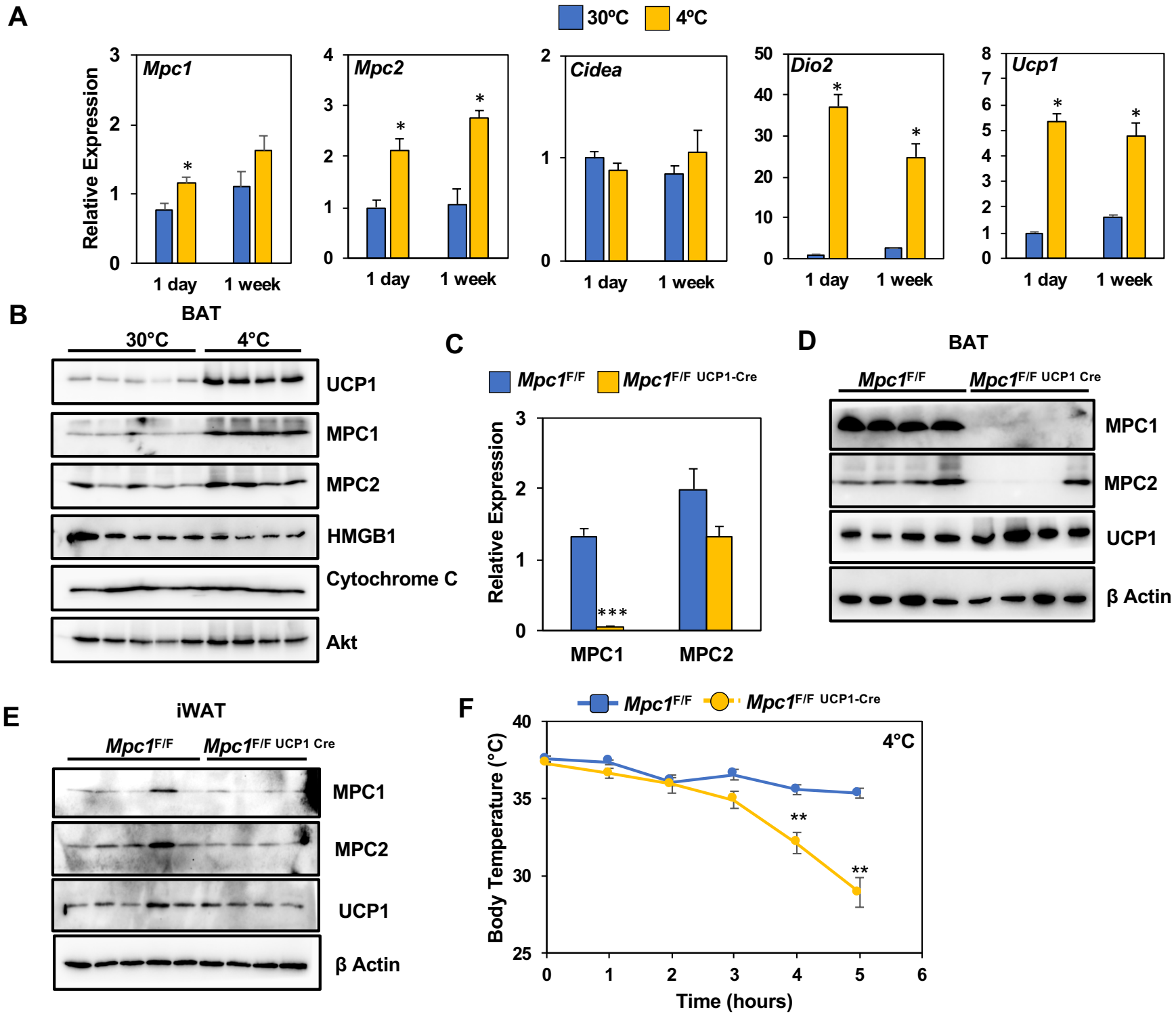
A
30ºC
4ºC
Relative Expression
Mpc1
Mpc2
Cidea
Dio2
Ucp1
1 day
1 week
B
BAT
30°C
4°C
UCP1
MPC1
MPC2
HMGB1
Cytochrome C
Akt
C
Mpc1F/F
Mpc1F/F UCP1-Cre
Relative Expression
***
MPC1
MPC2
D
BAT
Mpc1F/F
Mpc1F/F UCP1 Cre
MPC1
MPC2
UCP1
β Actin
E
iWAT
Mpc1F/F
Mpc1F/F UCP1 Cre
MPC1
MPC2
UCP1
β Actin
F
Mpc1F/F
Mpc1F/F UCP1-Cre
4°C
Body Temperature (°C)
Time (hours)
**
**

Figure 3

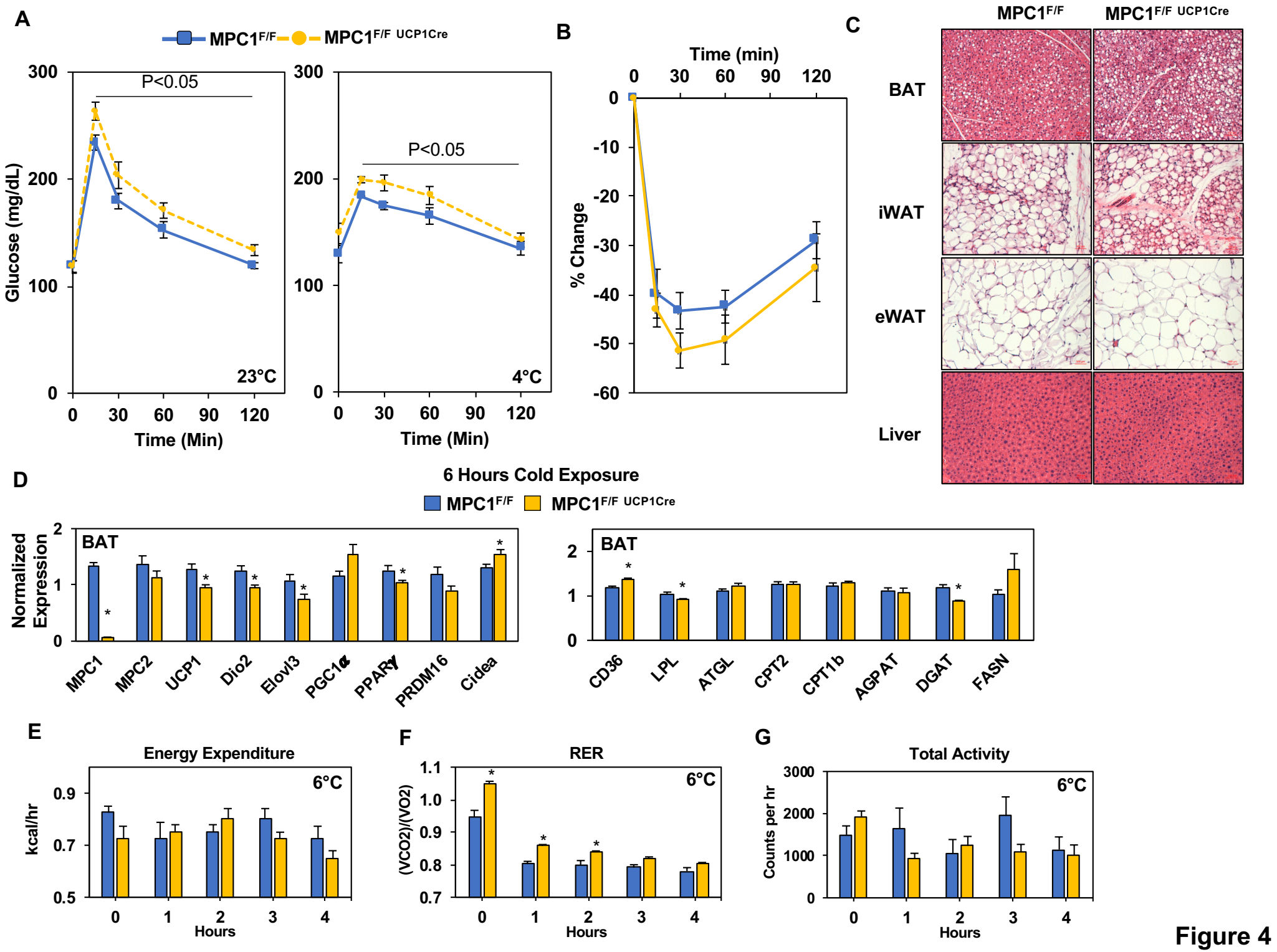
A
MPC1F/F
MPC1F/F UCP1Cre
Glucose (mg/dL)
P<0.05
23°C
4°C
Time (Min)
B
Time (min)
% Change
C
MPC1F/F
MPC1F/F UCP1Cre
BAT
iWAT
eWAT
Liver
D
6 Hours Cold Exposure
Normalized Expression
MPC1
MPC2
UCP1
Dio2
Elovl3
PGC1α
PPARγ
PRDM16
Cidea
CD36
LPL
ATGL
CPT2
CPT1b
AGPAT
DGAT
FASN
E
Energy Expenditure
kcal/hr
F
RER
(VCO2)/(VO2)
G
Total Activity
Counts per hr
Hours

Figure 4

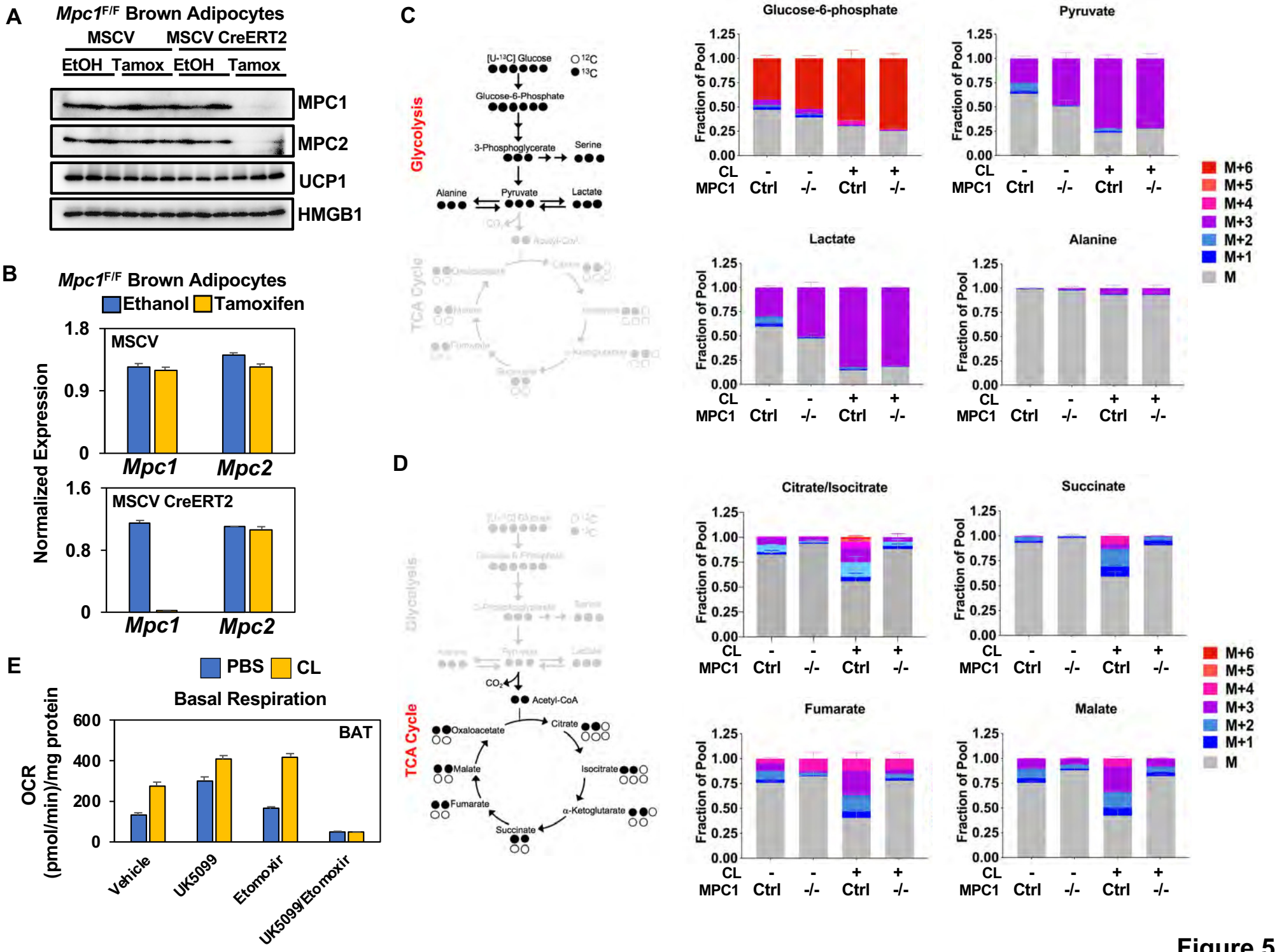
A
Mpc1F/F Brown Adipocytes
MSCV
MSCV CreERT2
EtOH
Tamox
EtOH
Tamox
MPC1
MPC2
UCP1
HMGB1
B
Mpc1F/F Brown Adipocytes
Ethanol
Tamoxifen
Normalized Expression
MSCV
MSCV CreERT2
Mpc1
Mpc2
C
Glycolysis
TCA Cycle
[U-13C] Glucose
12C
13C
Glucose-6-Phosphate
3-Phosphoglycerate
Serine
Alanine
Pyruvate
Lactate
Glucose-6-phosphate
Pyruvate
Lactate
Alanine
Fraction of Pool
CL
MPC1
Ctrl
-/-
M+6
M+5
M+4
M+3
M+2
M+1
M
D
Citrate/Isocitrate
Succinate
Fumarate
Malate
CO2
Acetyl-CoA
Citrate
Isocitrate
α-Ketoglutarate
Succinate
Fumarate
Malate
Oxaloacetate
E
PBS
CL
Basal Respiration
BAT
OCR
(pmol/min)/mg protein
Vehicle
UK5099
Etomoxir
UK5099/Etomoxir

Figure 5

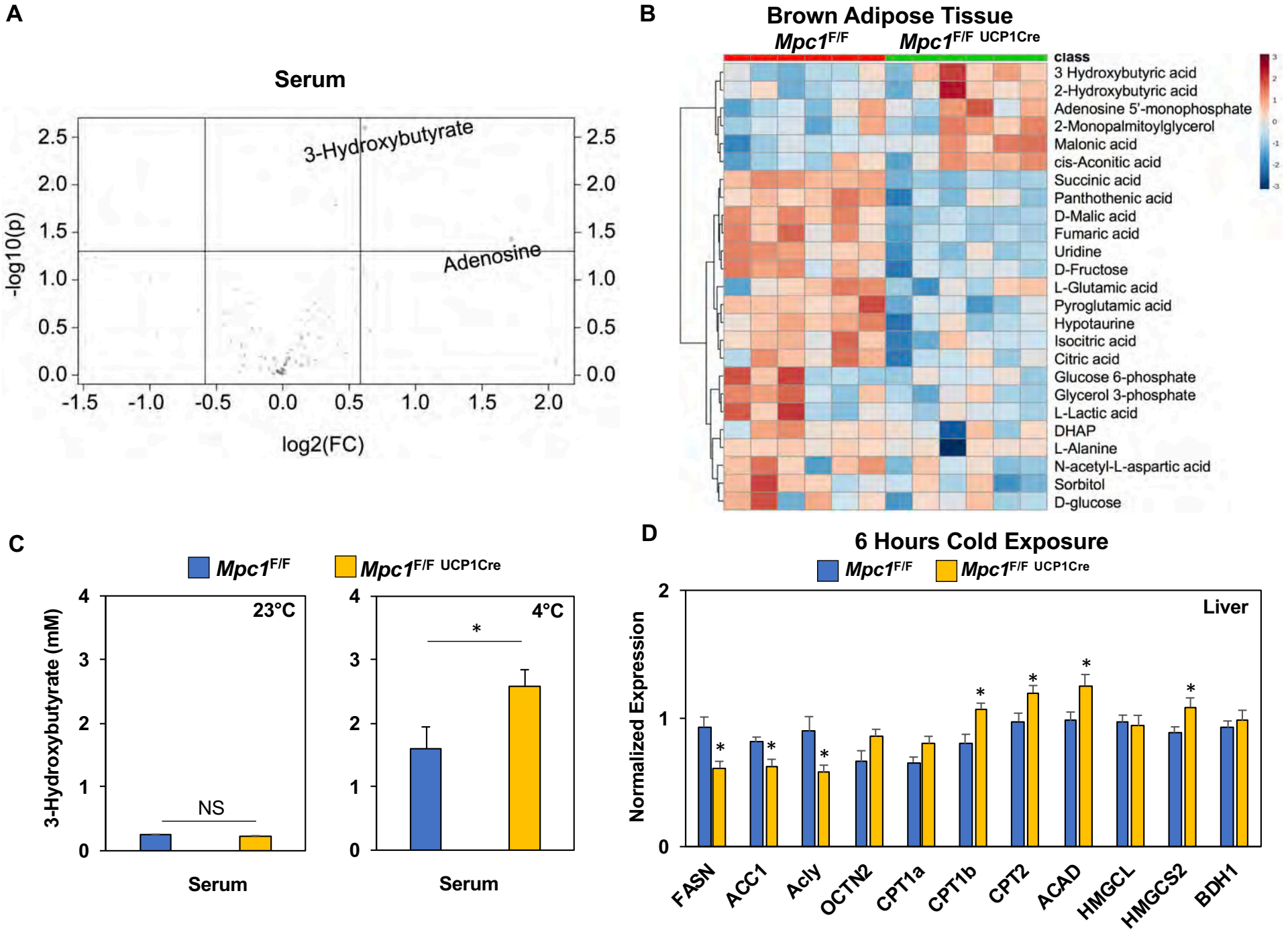
A
Serum
3-Hydroxybutyrate
Adenosine
-log10(p)
log2(FC)
B
Brown Adipose Tissue
Mpc1F/F
Mpc1F/F UCP1Cre
class
3 Hydroxybutyric acid
2-Hydroxybutyric acid
Adenosine 5'-monophosphate
2-Monopalmitoylglycerol
Malonic acid
cis-Aconitic acid
Succinic acid
Panthothenic acid
D-Malic acid
Fumaric acid
Uridine
D-Fructose
L-Glutamic acid
Pyroglutamic acid
Hypotaurine
Isocitric acid
Citric acid
Glucose 6-phosphate
Glycerol 3-phosphate
L-Lactic acid
DHAP
L-Alanine
N-acetyl-L-aspartic acid
Sorbitol
D-glucose
C
Mpc1F/F
Mpc1F/F UCP1Cre
23°C
4°C
NS
3-Hydroxybutyrate (mM)
Serum
Serum
D
6 Hours Cold Exposure
Mpc1F/F
Mpc1F/F UCP1Cre
Liver
Normalized Expression
FASN
ACC1
Acly
OCTN2
CPT1a
CPT1b
CPT2
ACAD
HMGCL
HMGCS2
BDH1

Figure 6

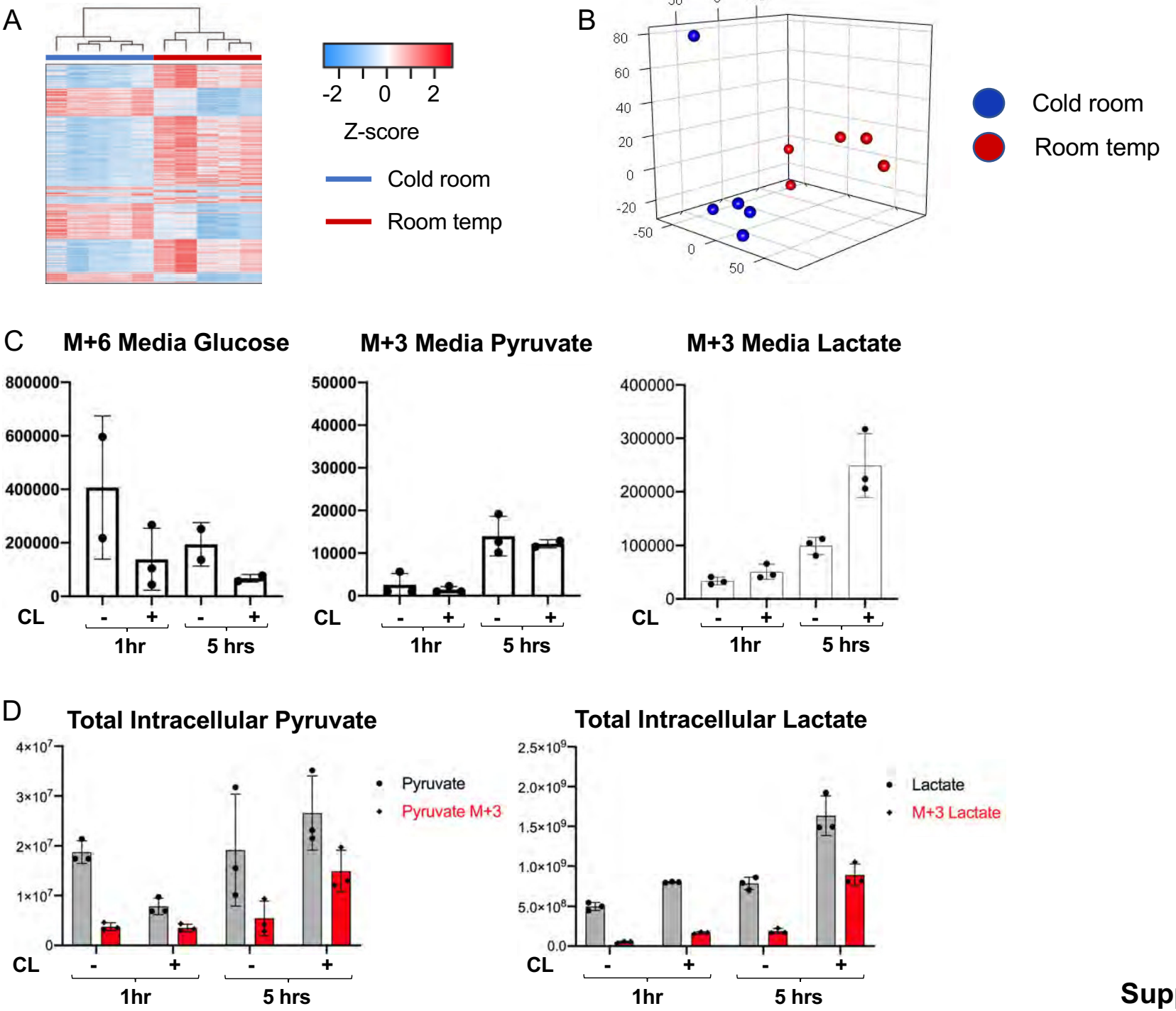


**Supplement Figure 1**

A

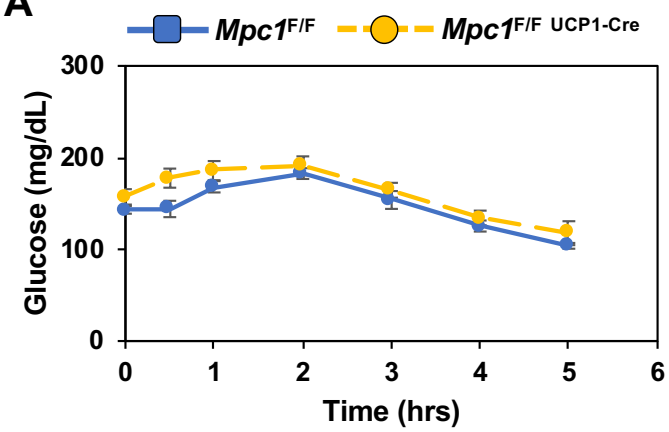


**Supplement Figure 3**

**Supplement Figure 3**

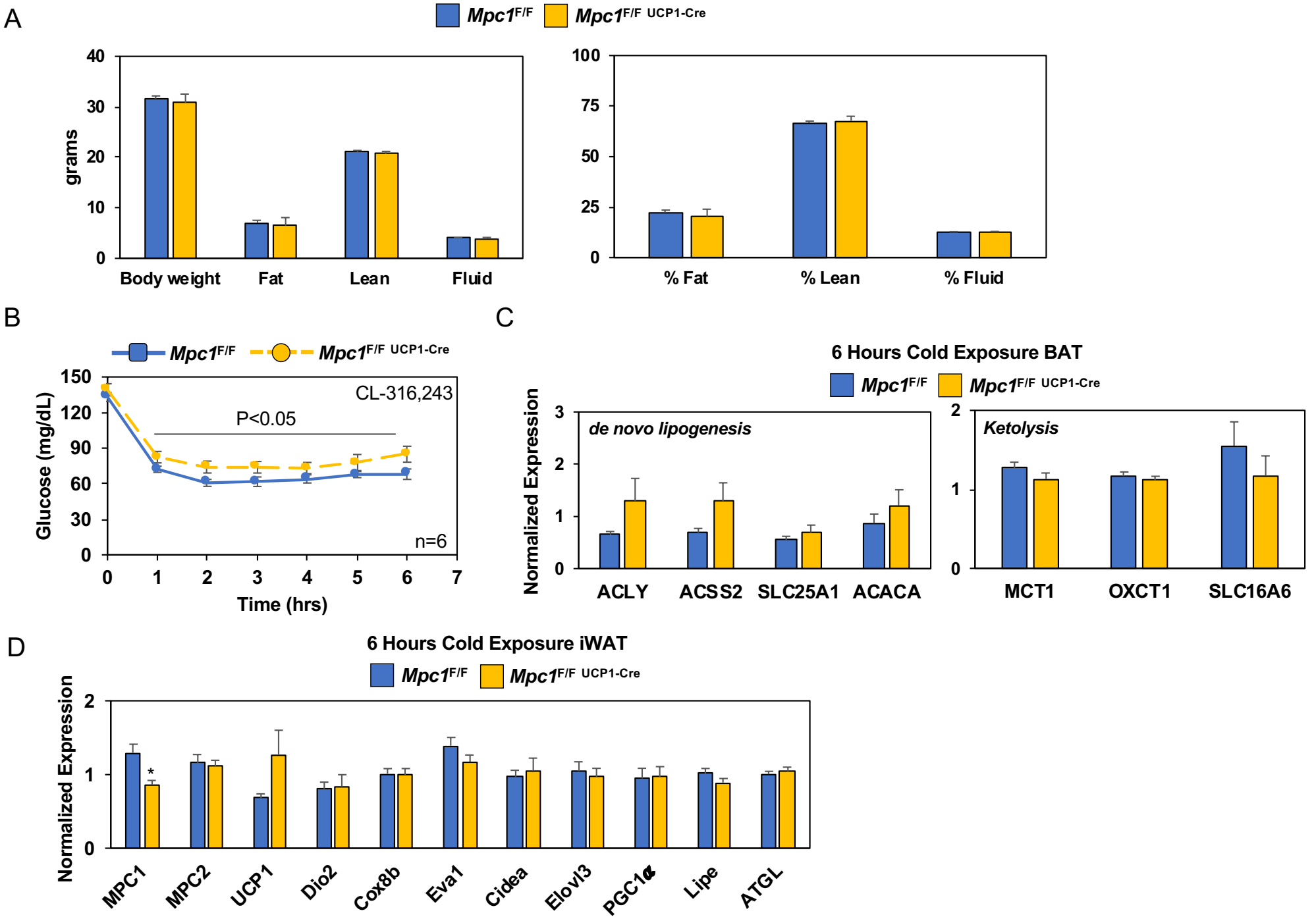

## Supplement Figure 4

A

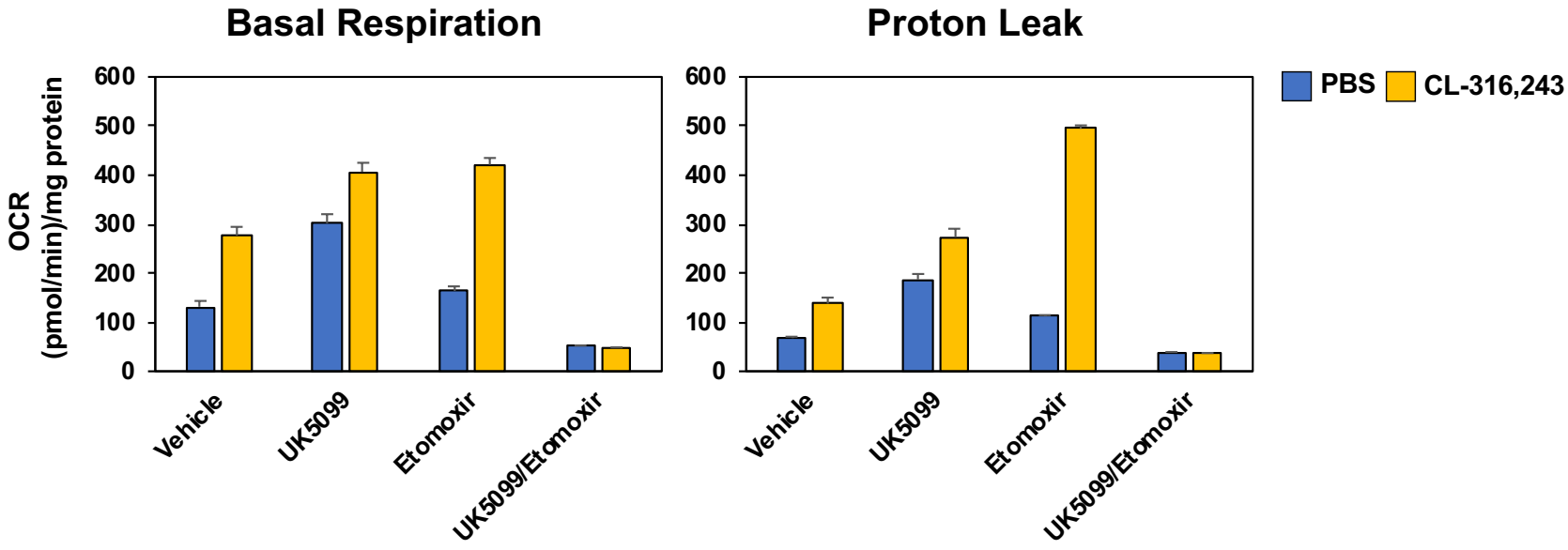


B

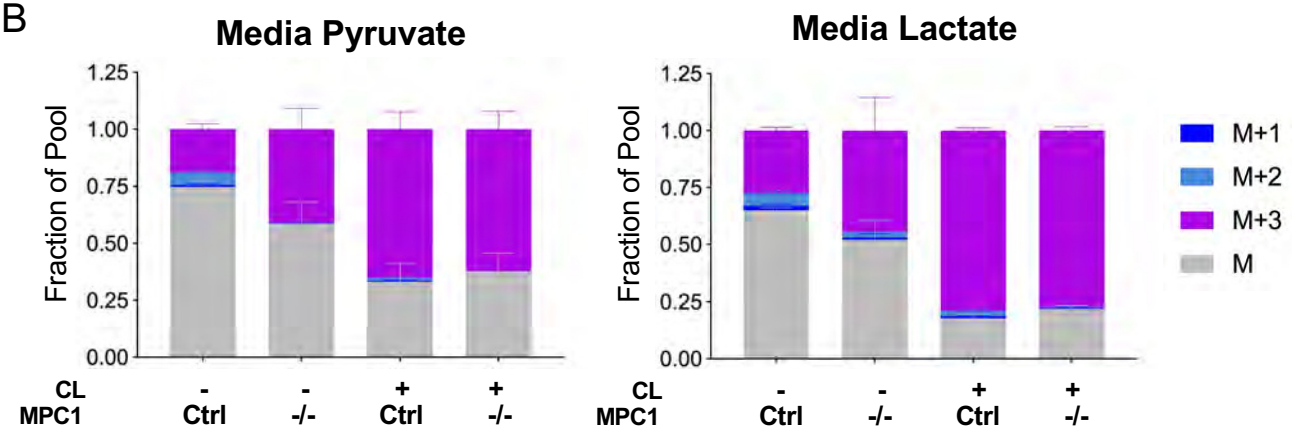

A

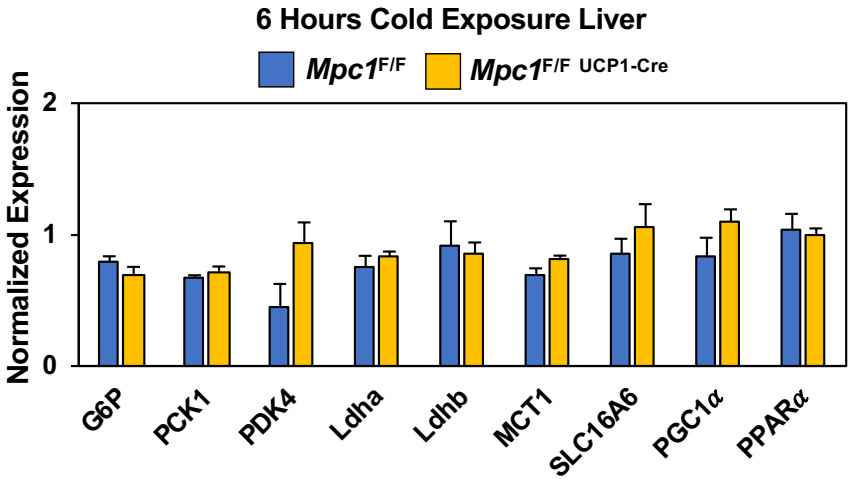


B

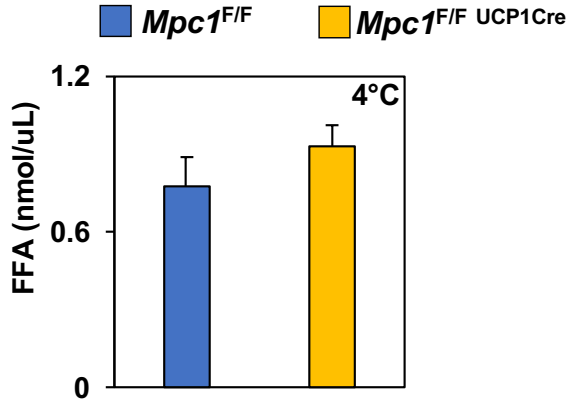


C

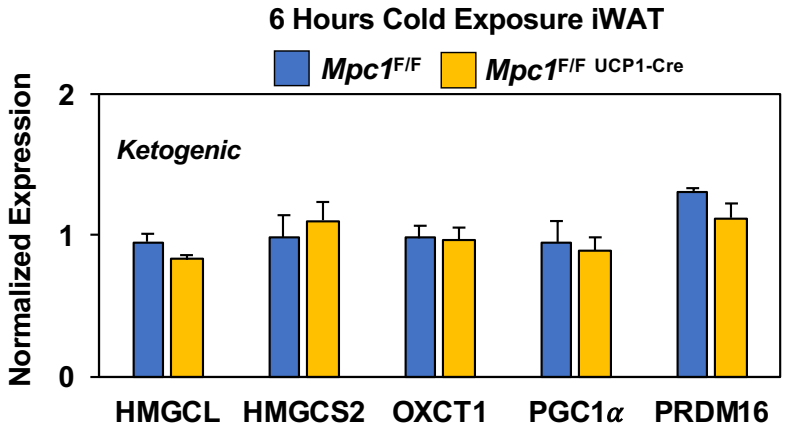


**Supplement Figure 5**